[American Journal of Science, Vol. 307, April, 2007, P. 678–708, DOI 10.2475/04.2007.02]

NEAR-SURFACE HYDROLOGIC RESPONSE FOR A STEEP, UNCHANNELED CATCHMENT NEAR COOS BAY, OREGON: 1. SPRINKLING EXPERIMENTS

BRIAN A. EBEL*†, KEITH LOAGUE*, WILLIAM E. DIETRICH**, DAVID R. MONTGOMERY***, RAYMOND TORRES§, SUZANNE P. ANDERSON§§, and THOMAS W. GIAMBELLUCA‡

ABSTRACT. Sprinkling systems are frequently used to simulate rainfall for process-based investigations of near-surface hydrologic response without measuring or accounting for spatial variability. Data analyses from three sprinkling experiments at the Coos Bay 1 experimental catchment (CB1) demonstrate considerable spatial variability in sprinkling. Furthermore, simulated rainfall from sprinklers was found to be more heterogeneous than natural storms at CB1. Water balance calculations and evapotranspiration estimates indicate that evaporation of airborne droplets is a significant portion of applied sprinkling rates, although still less than the amount blown off the field site by strong winds. Incorporation of spatial variability in sprinkling input and soil-water storage did not significantly change water balance calculations. Saturation patterns within the near-surface soil profile and the timing of tensiometric response are affected by sprinkling heterogeneity. Pore-water pressure and saturation development at the soil-saprolite interface are primarily controlled by convergent surface / subsurface topography and bedrock fracture flow, but are also sensitive to sprinkling spatial variations. The analyses presented herein suggest that incorporating spatial variability in sprinkling rates is important when conducting hydrologic-response modeling of sprinkler experiments. This paper is the first-part of a two-part series focused on CB1. The data analyses in this paper are used to parameterize comprehensive physics-based hydrologic-response simulations of three CB1 sprinkling experiments reported in the companion paper.

INTRODUCTION

Landscape evolution, while driven by diverse physical, chemical, and biological processes, is often largely controlled by the actions of water on the surface and within the subsurface (Gilbert, 1877). With this in mind, the importance of near-surface hydrologic-response should not be underestimated when investigating geomorphic processes. At the same time, the spatial heterogeneity present in natural systems (for example, saturated hydraulic conductivity, soil / bedrock thickness, and topography) combined with temporal variations in precipitation intensity and duration make it difficult to quantitatively evaluate the relative influence of the different factors governing hydrologic processes. Using sprinkling systems to mimic precipitation facilitates controlling the temporal variations in rainfall, simplifying hydrologic-response analysis. The strong link between geomorphic and hydrologic processes motivated the controlled sprinkling experiments at the Coos Bay experimental catchment (CB1). The primary objectives of the CB1 study were to investigate the mechanisms responsible for pore-water pressure development and shallow subsurface runoff generation. Elevated pore-water pressures can reduce effective stresses, driving slope failure. It is worth noting that CB1 failed as a landslide in 1996 in response to a large

*Department of Geological and Environmental Sciences, Stanford University, Stanford, California 94305-2115
**Department of Earth and Planetary Science, University of California, Berkeley, California 94720-4767
***Department of Earth and Space Sciences, University of Washington, Seattle, Washington 98195
§Department of Geological Sciences, University of South Carolina, Columbia, South Carolina 29208
§§Institute of Arctic and Alpine Research, University of Colorado, Boulder, Colorado 80309-0450
‡Department of Geography, University of Hawaii at Manoa, Honolulu, Hawaii 96822
† Corresponding author: bebel32@pangea.Stanford.EDU

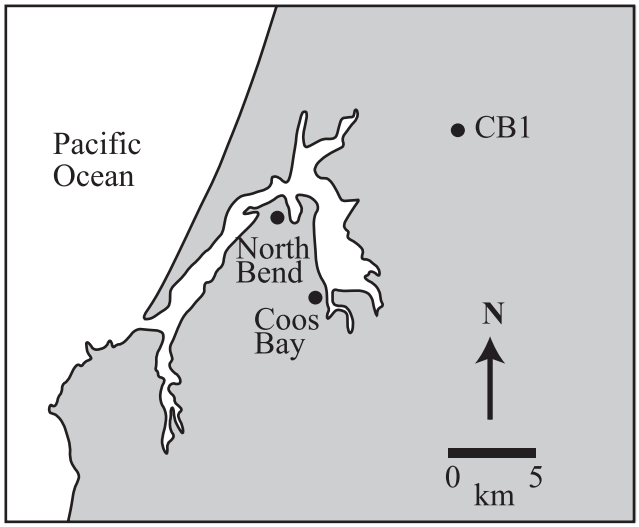

Fig. 1. Location map for the CB1 study area in the Oregon Coast Range.

storm (Montgomery and others, manuscript in preparation). To the best of the authors' knowledge, the CB1 measurements represent the most complete hydrologic-response data set available for any catchment that has failed.

The sprinkling experiments and long-term monitoring effort at CB1 (Montgomery, ms, 1991; Anderson, ms, 1995; Torres, ms, 1997) focused on producing a comprehensive dataset pertaining to hydrologic response. The published work from CB1 (Anderson and others, 1997a, 1997b, 2002; Montgomery and others, 1997, 2002; Torres and others, 1998; Anderson and Dietrich, 2001; Montgomery and Dietrich, 2002) has contributed to understanding the mechanisms of pore-water pressure development, subsurface runoff generation, and weathering in unchanneled valleys. This paper is the first of a two-part series focused on the CB1 catchment. The work reported herein evaluates the spatial variability in sprinkling and the observed effects on the CB1 hydrologic response. In the companion paper (Ebel and others, 2007), the hydrologic response from the three CB1 sprinkling experiments is simulated with a comprehensive physics-based model to better understand runoff and pore-water pressure generation. The data analyses and conclusions reported here provide both the foundation and the evaluation framework for the numerical modeling in the second paper.

CB1 STUDY AREA

Field-scale experiments designed to investigate hydrologically-driven landscape evolution, including slope failure, rely upon careful site selection where the critical factors include: (i) a manageably-sized site, (ii) accessibility, (iii) a tractable hydrologic and geomorphic boundary-value problem, and (iv) characteristics conducive to landslide initiation (for example, steep slopes, reduced root cohesion from logging). Figure 1 shows the location of the CB1 study area in the Oregon Coast Range near Mettman Ridge, 15 km northeast of the city of Coos Bay (OR). Figure 2 is a photograph of the 860 m^2 CB1 experimental catchment. CB1 is small enough to enable detailed monitoring of hydrologic response, yet it comprises the entire source area for a first-order stream. Logging roads in the Mettman Ridge area provided access to the site. The logging landing at the ridge top allowed for the storage of water in large

Fig. 2. Photograph of CB1 showing stairs / platforms, water tank, piezometers, shed that housed the TDR multiplexer, and a landslide scar in the adjacent hollow (bottom left).

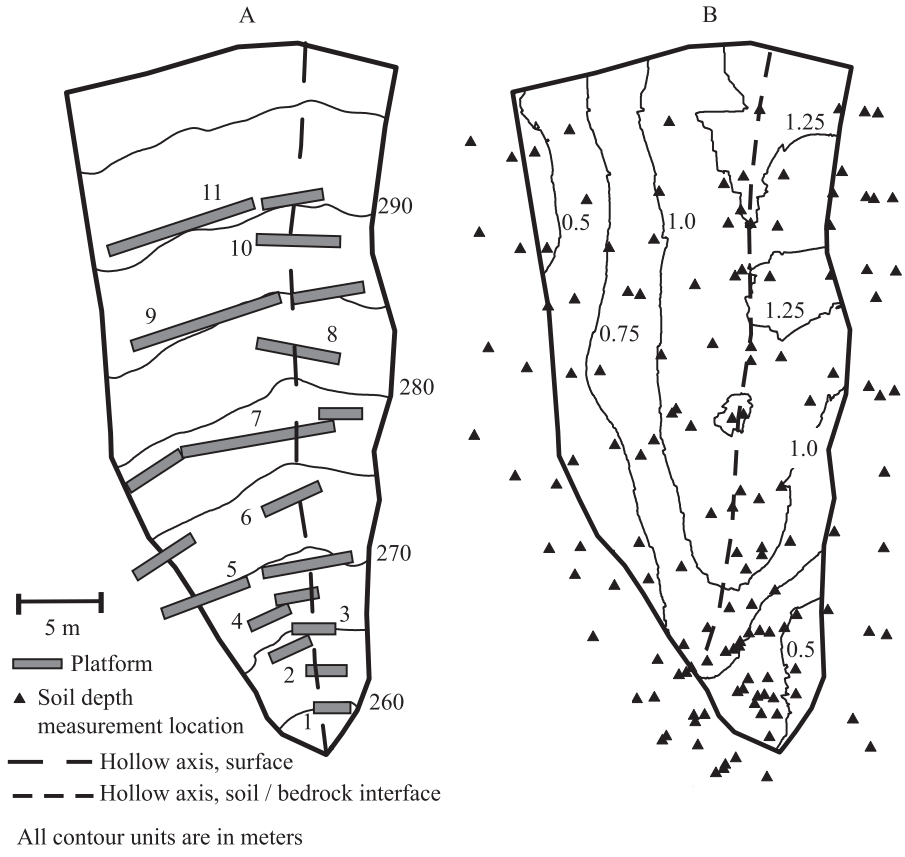

Fig. 3. (A) Contour map of the surface topography showing the surface hollow axis and the wooden platform network used to install and monitor the CB1 instrumentation. (B) Contour map of the CB1 soil depth and the hollow axis of the soil-saprolite interface.

holding tanks that facilitated using the topographic relief to drive sprinklers that mimic rainfall. Figure 3A shows a contour map of the steep (~43° slope) surface topography and surface topography hollow axis at CB1 based on the detailed theodalite survey from Montgomery and others (1997). Figure 3B shows a contour map of the soil-saprolite interface topography and soil-saprolite interface hollow axis based on over 100 measurements from piezometer installation (Montgomery and others, 1997; Schmidt, ms, 1999). The mean annual rainfall at the nearby North Bend (OR) airport, based on 29 years of data, is ~1.6 m yr^{-1} (Taylor and others, 2005). The old growth coniferous forest at CB1 was removed by a fire ~100 years ago. The second growth forest was logged by clear-cutting methods in February and March, 1987, treated with an application of a broadleaf herbicide (Roundup®) in July, 1988 (Torres, ms, 1997) to remove groundcover, and replanted with Douglas Fir (*Pseudotsuga menziesii*) seedlings in January, 1989 (Montgomery, ms, 1991). The broadleaf vegetation [Alder (*Alnus*) trees and blackberry (*Rubus*) vines] was periodically trimmed at the site from 1990 through 1992; the vegetation was not cut after 1992. The current state of vegetation at the site consists of Douglas Fir (*Pseudotsuga menziesii*) trees from 5 to 8 meters in height (see picture in Ebel and Loague, 2006) with undergrowth consisting

Table 1

Summary of CB1 sprinkling experiments (after table 2 from Anderson and others, 1997b)

Experiment	Dates	Intended sprinkling rate (mm h^{-1})	Experiment duration (h)	Intended total sprinkling (mm)
1	May 8-14, 1990	1.5	142	213
2	May 23-27, 1990	3.0	97	291
3	May 27-June 3, 1992	1.65	166	274

of Alder (*Alnus*), sword fern (*Polystichum munitum*), and bramble (*Rubus*). Table 1 summarizes the three sprinkling and tracer experiments conducted at CB1. Figure 4 is a map of the CB1 instrumentation that facilitates a detailed characterization of hydrologic-response (Anderson and others, 1997b; Montgomery and others, 1997; Torres and others, 1998). Thirteen rotating Rainbird® sprinklers (fig. 4) mounted 2 m above the ground were regulated using a system of pressure valves and gauges adjusted to maintain the flow rates. A 38,000 L storage tank for experiment 3 (15,000 L in experiments 1 and 2) located at the ridge crest (fig. 2) supplied water to the sprinklers through a pipe network. The tank was refilled using a 4,000 L tanker truck that transported water from a quarry pond 2 km away. The experiment 1 and 3 intended irrigation rates (table 1) represent <1 year 24 hour recurrence interval storms. The experiment 2 irrigation rate (table 1) represents a 1 to 2 year 24 hour recurrence interval storm. Both recurrence intervals are based on the North Bend and Alleghany (OR) rainfall records spanning, respectively, 23 and 41 years (Montgomery and others, 1997).

Table 2 provides information on the spatial and temporal distribution of the hydrologic-response observations collected during the three sprinkling experiments (table 1). These observations (see table 2, fig. 4) were made at 148 manual rain gages, three automated tipping-bucket rain gages, 223 piezometers, 100 tensiometers, 42 time-domain reflectometry (TDR) waveguide pairs, and 34 lysimeters (Anderson and others, 1997a, 1997b; Montgomery and others, 1997; Torres and others, 1998). Figure 3A shows the suspended wooden platforms that the instrumentation in figure 4 was emplaced and monitored from. Seepage from subsurface flow at CB1 was monitored at two v-notch weirs equipped with stage-height recorders. The upper weir is located at the channel head and anchored to bedrock; plastic coated plywood sealed into the bedrock routes soil water into the flume. The lower weir, located approximately 15 m downslope from the upper weir, was installed during experiment 2 to capture the bedrock component of near-surface flow that was missing in the water balance from experiment 1. The upper weir recorded from January 1990 through November 1996; the lower weir recorded from October 1991 through November 1996.

Relative to the information necessary for investigating hydrologic-response via physics-based simulation (Ebel and others, 2007), the CB1 measurements provide topography, characteristics of the soil [thickness, saturated hydraulic conductivity (slug tests), soil-water content and porosity (TDR measurements), capillary pressure relationships (from plot experiments)], irrigation rates, meteorology data (collected from net radiometers, soil heat flux plates, anemometers, thermometers, and relative humidity sensors), discharge at the weirs, pressure head response in the near surface, tracer concentrations (from ceramic cup lysimeters, tension lysimeters, and plate lysimeters), and discharge chemistry.

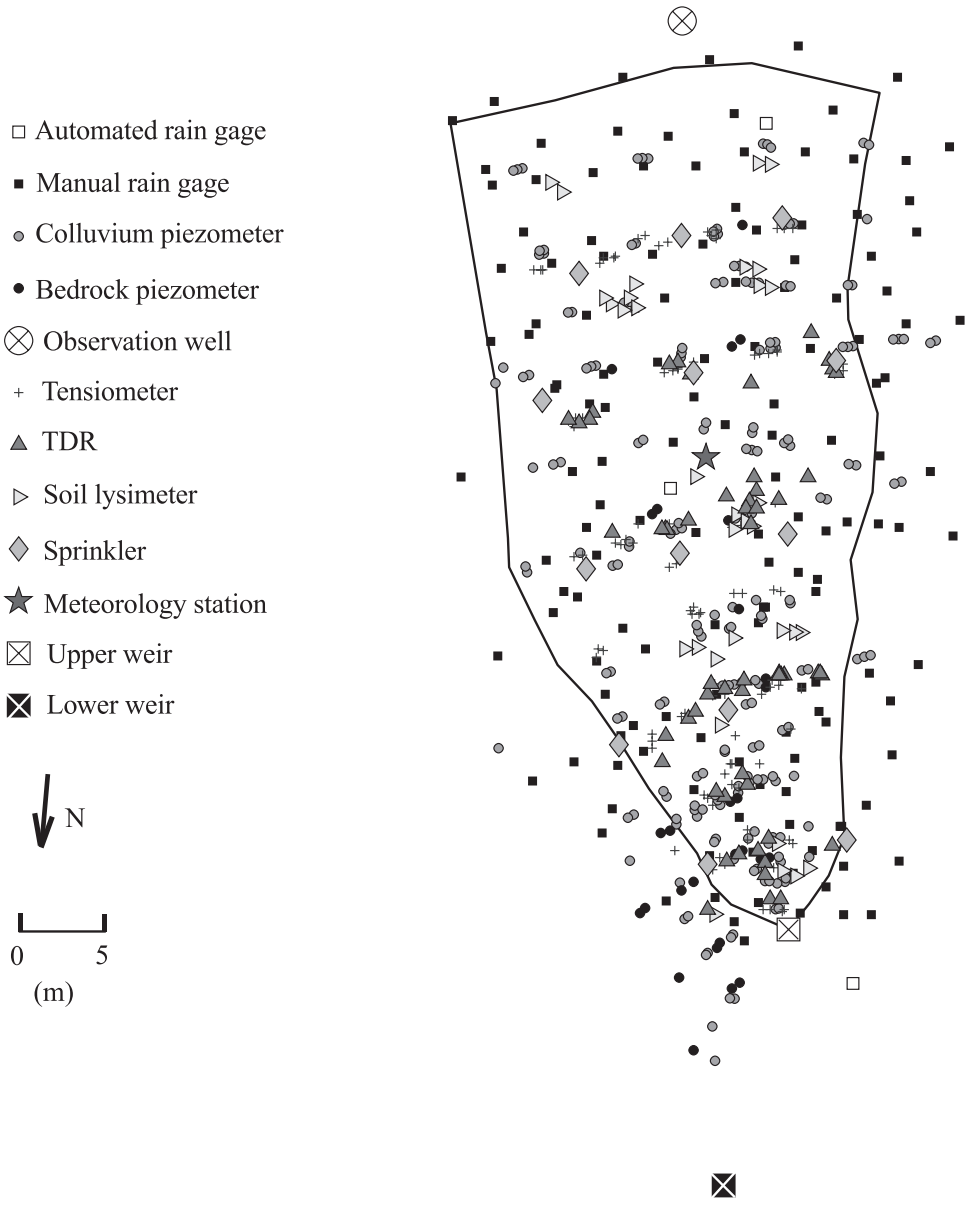

Fig. 4. Locations of the CB1 instrumentation (also see table 2).

RAINFALL SIMULATION

It is worth noting that "simulation" will be used in two contexts in this two-part paper. In this paper, rainfall simulation refers to using sprinkler systems to mimic natural rainfall. In the companion paper (Ebel and others, 2007), hydrologic-response simulation refers to the numerical solution of the coupled partial-differential equations that describe subsurface / surface water flow. The appeal of rainfall simulation was evident early on to hydrologists; for example, Robert Horton used sprinkling in

TABLE 2

Summary of hydrologic-response instrumentation monitored during the CB1 sprinkling experiments (see fig. 4).

Instrument[1]	Sprinkling experiment	Number of instruments	Temporal resolution (h)	Average horizontal spatial resolution (m)	Average vertical spatial resolution (m)	Depth range (m)
Automated rain gages	1, 2, 3	3	0.2	26.0[6], 16.9[8]-		
Manual rain gages	1, 2, 3	148	9-15	2.0[6], 2.5[8]	-	-
Upper weir	1, 2, 3	1	0.2	-	-	-
Lower weir	2, 3	1	0.2	-	-	-
Soil / saprolite piezometers	1, 2, 3	195	1-5[4], 0.2[5]	2.1[6, 7], 3.2[7, 8]	0.5	0.15-2.0
Bedrock piezometers	3	28	2-5[4], 0.2[5]	1.5[6, 7], 7.1[7, 8]	1-3	0.55-5.05
Tensiometers	1, 2, 3	100	1-2	2.6[6, 7], 5.0[7, 8]	0.25	0.16-1.25
TDR[2] waveguides	3	42	2	2.3[6, 7], 6.1[7, 8]	0.25	0.3-1.3
Lysimeters[3]	3	34	6-10	1.0[6], 5.0[7,8]	-	0.16-2.0
Meteorology instruments	3	1	0.3	-	-	-

[1]See figure 4 for CB1 instrument locations

[2]Time-domain reflectometry

[3]Three types of lysimeters were deployed at CB1. Readily mobile soil water (saturated soil) was sampled with zero-tension lysimeters while less mobile soil water (unsaturated soil) was sampled using plate and cup style lysimeters.

[4]Hand-recorded piezometers

[5]Automated piezometers

[6]Average horizontal spatial resolution defined as the mean separation distance between instrument locations and reflects the spatial resolution along the platforms where instruments were preferentially clustered

[7]Average horizontal resolution for nested instruments omits the small separation distances between instruments in the same nest and is indicative of the average spacing between nests

[8]Average horizontal spatial resolution, defined as $\sqrt{860m^2/N}$, where N is the number of instruments (or number of instrument nests)

TABLE 3

Selected characteristics and performance metrics for rainfall simulator experiments on large plots

Study	Site attributes		Statistics	
	Area (m^2)	Number of rain gages	CU (%)	CV (%)
Esteves and others (2000)	50	50	84[1]	16[1]
Motha and others (2002)	200	29	-	32[2]
Croke and others (1999)	300	20	-	7.8
Lane and others (2004)	450	20	-	10
Sumner and others (1996)	600	-	9	-
Luk and others (1993)	630	-	75	< 20
Riley and Hancock (1997)	1000	-	75-95	< 20
This study	860	148	60-75	31-50

[1]Mean of the values reported in table 4 of Esteves and others (2000)
[2]Mean of the values reported in table 1 of Motha and others (2002)

1914 to examine infiltration capacities (Wisler and Brater, 1959). A review of rainfall simulation studies from 1914 to 1969 is provided by Hall (1970). More recently, rainfall simulators have been employed in studies of hydrologic response (for example, Hornberger and others, 1991; Waddington and Devito, 2001; Sharpley and Kleinman, 2003) and erosion (for example, Parsons and others, 1998; Wilson, 1999; Motha and others, 2002). The advantages of controlling the sprinkling intensity and duration (as well as the solute input), to minimize temporal variability, do not come without the difficulties of reproducing natural rainfall characteristics (that is, spatially-uniform intensities, drop size distributions, and drop kinetic energies). Almost all rainfall simulator studies forgo rigorous analysis of the spatial variations in rainfall intensity (Lascelles and others, 2000). The effort reported herein compares spatial variations in intensity between simulated and natural storms and evaluates the effects of sprinkling heterogeneity on the observed CB1 hydrologic response.

Common Metrics of Rainfall Simulator Performance

Common metrics for evaluating the spatial uniformity of sprinkling include the coefficient of uniformity (CU), the coefficient of variation (CV), and the standard deviation (SD). The CU (Christiansen, 1942) is calculated, as a percentage, by:

$$\mathrm{CU} = 100\left(1 - \frac{\Sigma_N |D_i - \bar{D}|}{\Sigma_N D_i}\right) \tag{1}$$

where N is the number of observations, D_i are the observed data, and $\bar{D}$ is the mean of the observed data. The CV is the ratio of the SD to $\bar{D}$. There are no universal guidelines in the rainfall simulation literature for what constitutes acceptable values of CU, CV, or SD. However, depending on the plot size, Esteves and others (2000) suggest that CU values between 70 to 90 percent are acceptable. Agricultural research has found that over large fields, irrigation CU values range between 57 to 90 percent, with a mean of 71 percent (Ascough and Kiker, 2002). Table 3 is a summary of CU and CV values achieved by selected rainfall simulators at sites 50 m^2 or larger.

It is worth noting that the CU and CV, the benchmark measures of assessing spatial variability in sprinkling, are far from perfect. For example, the CU provides no information about the sprinkling pattern in that two completely different sprinkling

TABLE 4

Statistics of observed sprinkling and rainfall rates from manual rain gages[1] at CB1

Experiment number, observed storm date	Rate statistics			
	M (mm h^{-1})	SD (mm h^{-1})	Day M (mm h^{-1})	Night M (mm h^{-1})
1	1.47	0.73	1.01	1.64
2	2.83	0.92	2.54	2.97
3	1.56	0.87	1.38	1.69
5/21/1990	2.10	0.27	-	-
6/13/1992	5.39	0.85	-	-

[1]The locations of the manual rain gages are shown in figure 4.
M denotes the arithmetic mean, SD is the standard deviation.
All statistics for sprinkling events are statistically weighted to ensure that observations representing longer periods of time contribute proportionally to the statistics (for example, the shorter daytime manual rain gage observations are weighted less than the longer nighttime observations).

patterns can result in the same CU. Esteves and others (2000) compared CU and CV values with contour maps of intensity and found appreciable spatial variability, despite high values of CU and low values of CV (see table 3). Lascelles and others (2000) also used contour maps of sprinkling intensity to illustrate considerable spatial and temporal variability, despite CU values consistently greater than 70 percent.

Sprinkling Variability at CB1

The CB1 dataset is ideal for (i) assessing the spatial variations in irrigation intensity / depth, (ii) comparing the sprinkling variability with natural rain variability, and (iii) determining the effects of spatial variability in sprinkling intensity on near-surface hydrologic response. High spatial resolution characterization of the three CB1 sprinkling experiments is facilitated by the 148 wedge rain gages (fig. 4) that were monitored twice daily (~9:00 am and ~6:00 pm). Three automated tipping-bucket rain gages (fig. 4) recorded sprinkling rates every 10 minutes. Rates of sprinkling are calculated as the depths recorded in the manual gages divided by the time between gage readings. For this study, it is assumed that all rain gage levels were read at the same time. Given that it took 30 to 45 minutes to read all the gages and the time in between readings was greater than 10 hours, this assumption has a small effect on the accuracy of the observed rates.

Table 4 summarizes the statistics calculated using the manual-gage sprinkling rates (from the three experiments) and rainfall rates (from two storms). Comparison of the intended (table 1) and observed (table 4) mean sprinkling rates reveals that the mean observed and intended rates are close, with errors of 2 percent, 6 percent, and 6 percent for experiments 1, 2, and 3, respectively. The error in the observed versus intended rates was determined, as a percentage, by:

$$Error = 100\left(\frac{(I - O)}{I}\right) \tag{2}$$

where I is the intended sprinkling rate and O is the mean observed sprinkling rate. A clear diurnal signature is evident in table 4, with lower mean observed rates in the daytime compared to the nighttime. Anderson and others (1997a) observed a strong diurnal cycle in the observed CB1 sprinkling, with the nighttime data consistently exhibiting larger mean rates, larger maximum rates, and higher SD compared to the

TABLE 5

Statistics of observed sprinkling and rainfall totals from manual rain gages at CB1[1]

Experiment number, observed storm date	Depth statistics					
	CU (%)	CV (%)	Day CU (%)	Night CU (%)	Day CV (%)	Night CV (%)
1	61	47	60	61	48	47
2	75	31	75	75	31	31
3	60	50	59	60	49	52
5/21/1990	90	13	-	-	-	-
6/13/1992	91	16	-	-	-	-

[1]The locations of the manual rain gages are shown in figure 4.
CV is the coefficient of variation; CU is the coefficient of uniformity, calculated with equation (1).

daytime sprinkling rates. It is worth noting that a higher SD does not necessarily denote more spatially variable rainfall because the SD for similarly shaped distributions will be larger for the higher rate. A better characterization of the diurnal variability is provided by the CV and / or the CU. Table 5 summarizes the CU and CV values from the three sprinkling experiments and two natural storms. Perusal of table 5 illustrates that despite considerable differences in the diurnal mean sprinkling rate, there is little diurnal variation in the CV or the CU, indicating that the overall spatial variability changes little in response to diurnal factors.

Figure 5 contains a time series (during the third sprinkling experiment) of the mean sprinkling rate recorded in the three automated tipping-bucket rain gages (at a height of 1 – 1.5 m) and the wind velocities measured at CB1 (the anemometer was

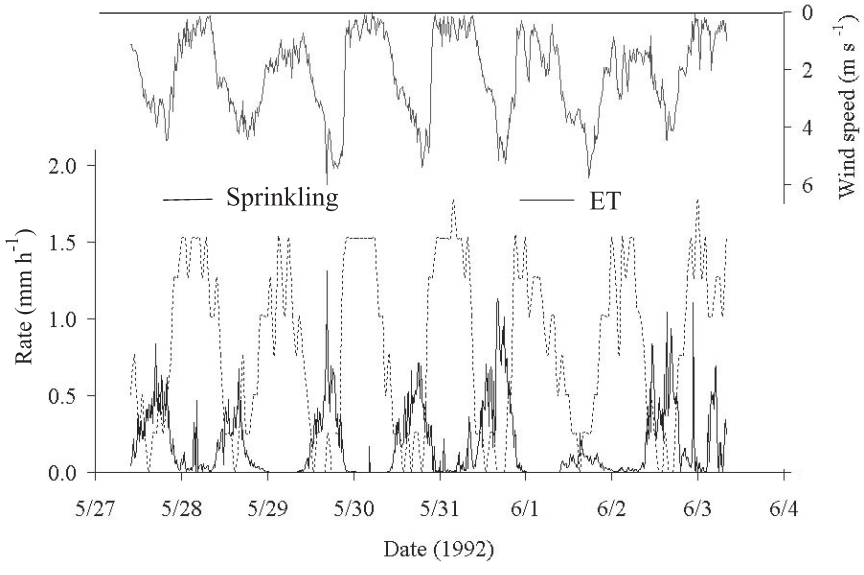

Fig. 5. Time series of observed wind speed, evapotranspiration estimated with the Penman-Monteith method, and the mean observed sprinkling rate from the three automated rain gages for sprinkling experiment 3.

positioned at a height of 3.0 m). The sprinklers are positioned at a height of 2.0 m. While the automated rain gages capture the overall temporal trends of sprinkling rates (fig. 5), the rates of sprinkling are inaccurate, with observed sprinkling rates approaching zero and total depths less than detected in nearby manual gages. Torres (ms, 1997) attributed the error in the automated gauge rates to the elevated gage heights (1 – 1.5 m), relative to the manual rain gages that are positioned 0.15 to 0.4 m above ground level. Rodda and Smith (1986) and Newson and Clarke (1976) found that elevated rain gages may result in undercatch because of droplet trajectories, with the undercatch enhanced by wind. Comparison of the wind speed and automated gage sprinkling rate time series (see fig. 5) suggests that wind enhances undercatch at the CB1 automated rain gages during the sprinkling experiments, which was also noted from observations during the sprinkling experiments (see Montgomery, ms, 1991; Torres, ms, 1997).

The CB1 values of CU and CV (shown in table 5) are equivalent (75% for experiment 2) to slightly less uniform (61 and 60%, for experiments 1 and 3, respectively) than those of Luk and others (1993) and Riley and Hancock (1997) for similarly sized areas (table 3). It is worth noting the steep terrain of CB1 (fig. 3A) makes uniform sprinkling difficult because of large head differences in the sprinkler lines. The CU and CV values in table 5 also indicate that higher sprinkling rates resulted in a more uniform (higher CU and lower CV) spatial distribution of sprinkling depths. The spatial uniformity decreases with increasing sprinkling rate for most rainfall simulators (for example, Esteves and others, 2000), or does not vary at all (Loch and others, 2001). The increase of uniformity with sprinkling rate at CB1 likely reflects a decline in pressure at the sprinkler nozzle with increasing sprinkling rate. Lower nozzle pressures produce fewer fine droplets and mist (Kincaid, 1996; Tarjuelo and others, 2000), resulting in less wind-driven alteration of the sprinkling pattern.

While the CU and CV offer some measure of the spatial variability in sprinkling intensity, explicit spatial analysis (for example, contour maps of sprinkling intensity) offers greater insight into the spatial structure (Lascelles and others, 2000). Figure 6 shows selected snapshots of intensity (using Ordinary Kriging with an exponential variogram model with a nugget to interpolate between gages) for the most variable (MV), least variable (LV), and the closest to the intended (CI) sprinkling rate for the three sprinkling experiments. The MV was defined as having the highest standard deviation and highest maximum rate; the LV was defined as having the smallest CV. These metrics were the most consistent with qualitative visual interpretations of sprinkling heterogeneity. The nine snapshots of sprinkling intensity (fig. 6) represent only a small fraction of the sprinkling data at CB1 with 12, 8, and 14 snapshots available for experiments 1, 2, and 3, respectively. The LV sprinkling snapshots in figure 6 exhibit considerable spatial variability. The MV snapshots in figure 6 have hotspots higher than the intended sprinkling rates. For the CI rate snapshots in figure 6, the differences between the mean observed sprinkling rates and the intended sprinkling rates (table 1) are only 0.01, 0.1, and 0.05 mm h^{-1} for experiments 1, 2, and 3, respectively. However, despite the small differences between the mean observed and intended sprinkling rates, it is clear from figure 6 that spatial variability is present. Figure 6 shows that the spatial structure in the sprinkling rates is strongly determined by the sprinkler locations, with higher rates near the sprinklers and lower rates near the CB1 perimeter.

Comparison of Natural Rain to Sprinkling

Rainfall rate observations made at the 148 manual gages for two natural storms at CB1, on 5/21/1990 (between sprinkling experiments 1 and 2, with a duration of 8 hours) and 6/13/1992 (immediately after sprinkling experiment 3, with a duration of 3 hours), facilitate comparing the spatial variability in natural rainfall intensity to

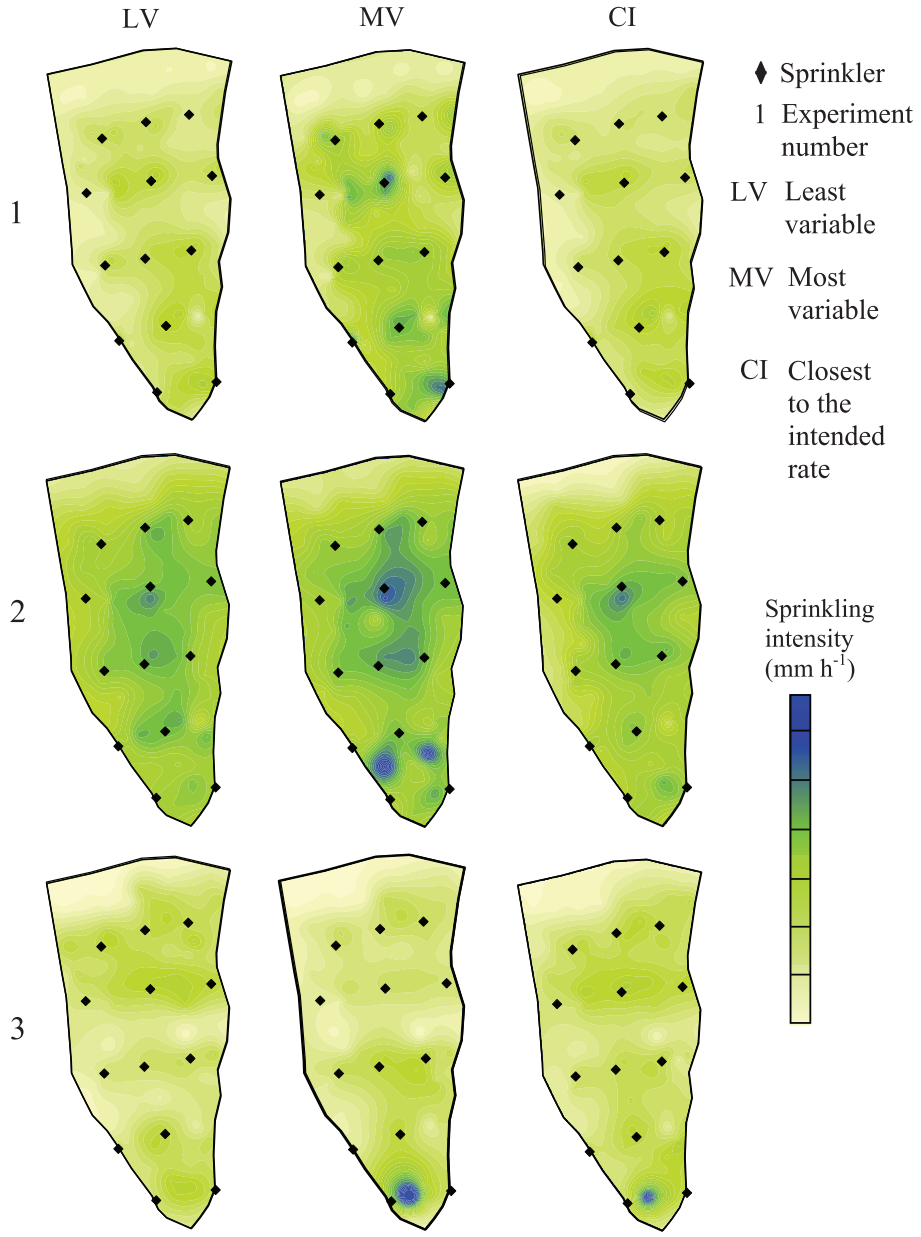

Fig. 6. Kriged snapshots of observed sprinkling rates for experiments 1, 2, and 3 representing the least variable (LV, the smallest CV), most variable (MV, the highest standard deviation and maximum sprinkling rate), and the closest to the intended sprinkling rate (CI, the mean observed sprinkling rate closest to the intended sprinkling rate).

simulated rainfall intensity. Perusal of the CU and CV values from table 5 and SD values from table 4 for simulated and natural rain reveals that the natural rainfall is more spatially uniform than the sprinkling. It is also worth noting that natural rain augmented sprinkling on the last day of experiment 2, increasing the CU and lowering the

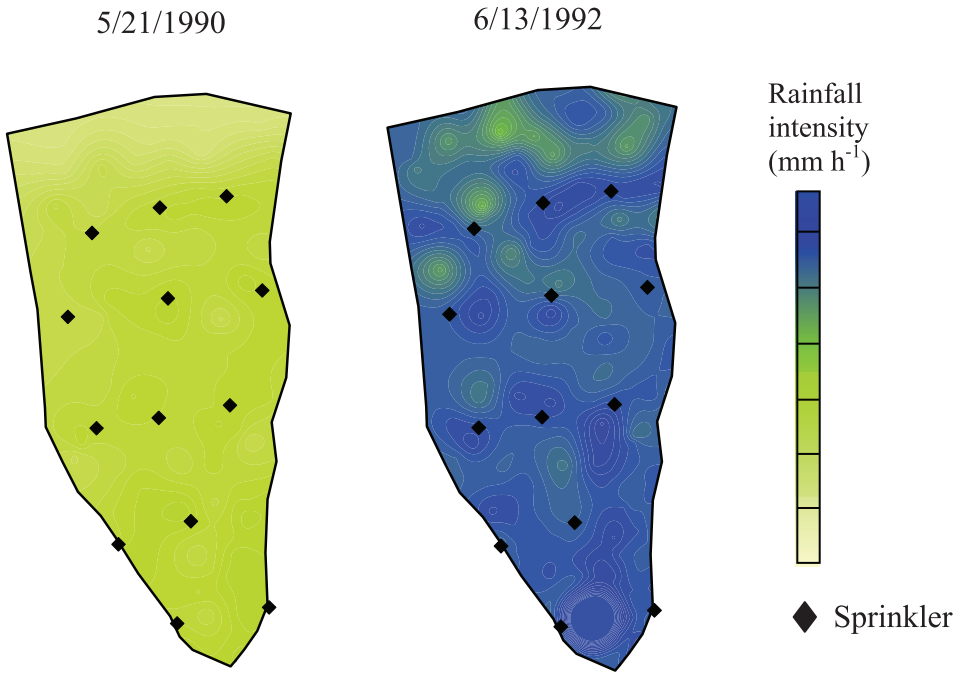

Fig. 7. Kriged snapshots of observed rainfall rates from the storms on 5/21/1990 and 6/13/1992.

CV (table 4), further highlighting the spatial uniformity of natural rain in comparison to rainfall simulators. The natural storms on 5/21/1990 and 6/13/1992 were the only rainfall events where rainfall rates were recorded in the manual gages at CB1, and only one sweep of the gages was conducted for each of these storms.

Figure 7 shows Kriged snapshots of the two natural storm rainfall rates, illustrating the differences in spatial variability between natural (fig. 7) and simulated (fig. 6) rainfall. In both natural storms (fig. 7), an area of lower intensity near the ridge crest exists, although it is less prominent than in the sprinkling experiments. The hotspot near the downgradient end of CB1 for sprinkling experiments 2 and 3 (fig. 6) also exists in the 6/13/1992 rainfall snapshot (fig. 7). Observations during the sprinkling experiments suggest that this persistent hotspot is the result of untrimmed broadleaf vegetation focusing sprinkling / rainfall into one rain gage (Torres, ms, 1997). As one would expect, the areas of higher intensity near the sprinklers in figure 6 are not noticeable in figure 7 for the natural storms. Figures 6 and 7 illustrate persistent spatial features (isolated hotspots, areas of lower intensity), present in the sprinkling that are not present in natural rainfall.

Examining omnidirectional experimental variograms from sprinkling and rainfall rates observed at CB1 provides a meaningful quantitative evaluation of the spatial continuity and structure. Figures 8A and 8B show the experimental variograms of sprinkling rates for snapshots during experiment 2 (fig. 8A) and experiment 3 (fig. 8B). The experimental variogram from the natural storm on 6/13/1992 is shown in figure 8C. All the variograms in figure 8 are standardized by the respective variances, making the sill equal to one. Examination of the sprinkling variograms (figs. 8A and 8B) shows that the sill is reached at a lag (or range) of 10 m (approximately the separation distance between sprinklers), illustrating the control of the sprinkler placements on spatial variations in intensity. The upward spikes in the sprinkling

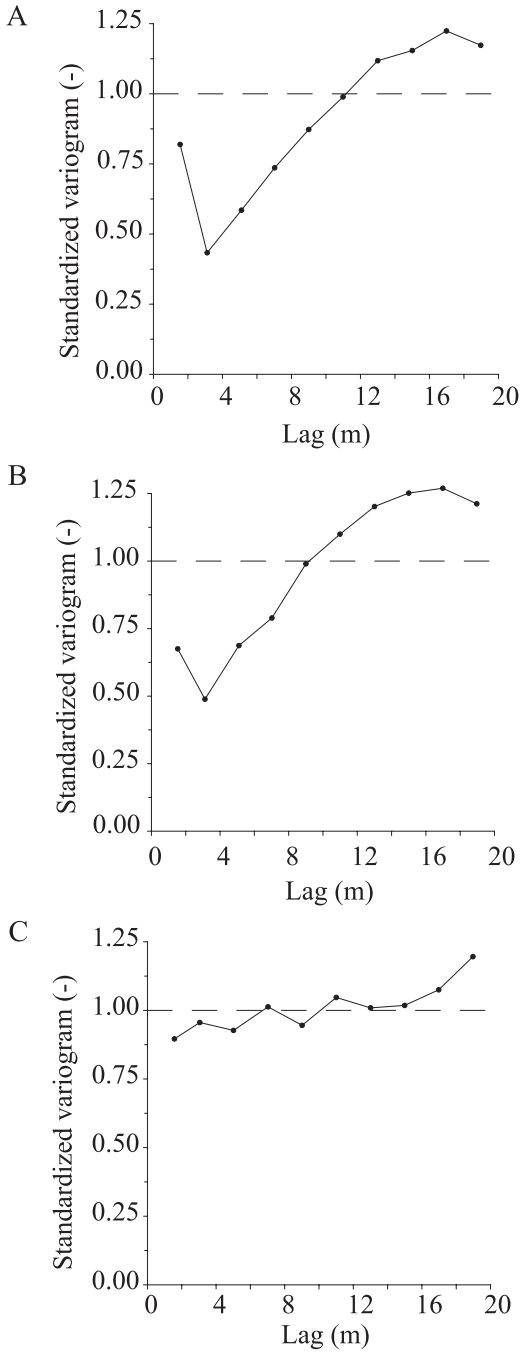

Fig. 8. (A) Experimental variogram from a sprinkling rate snapshot at 5:20 PM on 5/24/1990 during experiment 2. (B) Experimental variogram from a sprinkling rate snapshot at 8:00 AM on 5/28/1992 during experiment 3. (C) Experimental variogram from the natural storm rates on 6/13/1992.

semivariograms at the 2 m lag are artifacts of having few data points at small lags. The parabolic shape of the semivariograms in figures 8A and 8B shows that there is considerable structure in the sprinkling intensity data. The nearly flat semivariogram for the natural rain in figure 8C shows no spatial structure.

Water Balance Contribution

Previous studies at CB1 (Anderson, ms, 1995; Montgomery and others, 1997; Torres, ms, 1997) have included water balances, assuming spatially and temporally constant sprinkling rates in the estimation of the volume of applied water during the three sprinkling experiments. Figures 9A, 9C, and 9E (for experiments 1, 2, and 3, respectively) show Kriged maps of the cumulative observed sprinkling depth (in the 148 gages). The colored contour lines in figures 9A, 9C, and 9E mark the intended depth for each experiment (see table 1 and the scale bar in fig. 9A). Figures 9B, 9D, and 9F (for experiments 1, 2, and 3, respectively) show the deviation between the intended depth (table 1) and the Kriged depths (figs. 9A, 9C, and 9E). The maps in figure 9 facilitate examining the effect of sprinkling spatial variability on the estimated volume of applied water for the water balance. Figures 9A, 9C, and 9E further illustrate the sprinkling spatial structure, with the areas near the sprinklers receiving at or well above the intended amount of water while areas at the catchment edges, particularly near the ridge crest, receive less water. The deviations between intended and observed depths shown in figures 9B, 9D, and 9F are encouraging in that the majority of the catchment receives within 50 mm of the intended sprinkling depth (table 1). However, inspection of figures 9B, 9D, and 9F shows that some portions of the catchment receive hundreds of mm above / below the intended sprinkling depth. Integration (sprinkling depth multiplied by the area at each Kriged grid cell) of the Kriged sprinkling depths in figures 9A, 9C, and 9E shows some discrepancy in the total volume applied between the intended and Kriged observed volumes. For experiment 1, the intended total applied volume was 182.8 m^3 and the integrated observed volume was 168.8 m^3 for a difference of 14 m^3 (8%). For experiment 2, the intended total applied volume was 250.3 m^3 and the integrated observed volume was 229.7 m^3 for a difference of 20.6 m^3 (9%). For experiment 3, the intended total applied volume was 235.6 m^3 and the integrated observed volume was 215.0 m^3 for a difference of 20.6 m^3 (10%). The implications of using the intended sprinkling depths, rather than the integrated observed sprinkling depths, in the water balance are discussed further in later sections.

EVAPOTRANSPIRATION ESTIMATES

A micrometeorology mast (fig. 4) was installed at CB1 before experiment 3 and monitored from 5/19/1992 through 6/8/1992 for estimating evapotranspiration (ET). The meteorological instruments included a net radiometer, soil heat flux plate, anemometers, thermometers, and relative humidity sensors that were each sampled every 5 seconds with mean values recorded every 15 minutes. Net radiation (horizontal and slope-parallel) and soil heat flux (slope-parallel) were measured at 2.0 m above the surface and 0.03 m below the surface, respectively. Wind speed (slope parallel) at 2.3 and 3.0 m, relative humidity at 3.1 and 4.1 m, and air temperature at 2.0, 3.1, and 4.1 m were also measured. It is worth noting that the meteorological instruments at CB1 were oriented to estimate ET fluxes perpendicular to the surface. Any calculation of the volumetric ET rate should use the surface area, which is the planimetric area corrected for the slope by dividing by the cosine of the slope angle (43°). Sprinkling and rainfall measurements are observed horizontally and volumetric fluxes are calculated using the planimetric area (860 m^2).

Alder (*Alnus*) trees and blackberry (*Rubus*) vines were cut from the site prior to the third sprinkling experiment to minimize sprinkling interception and evapotranspiration. Because there was only one meteorological mast at CB1, the spatial variability in

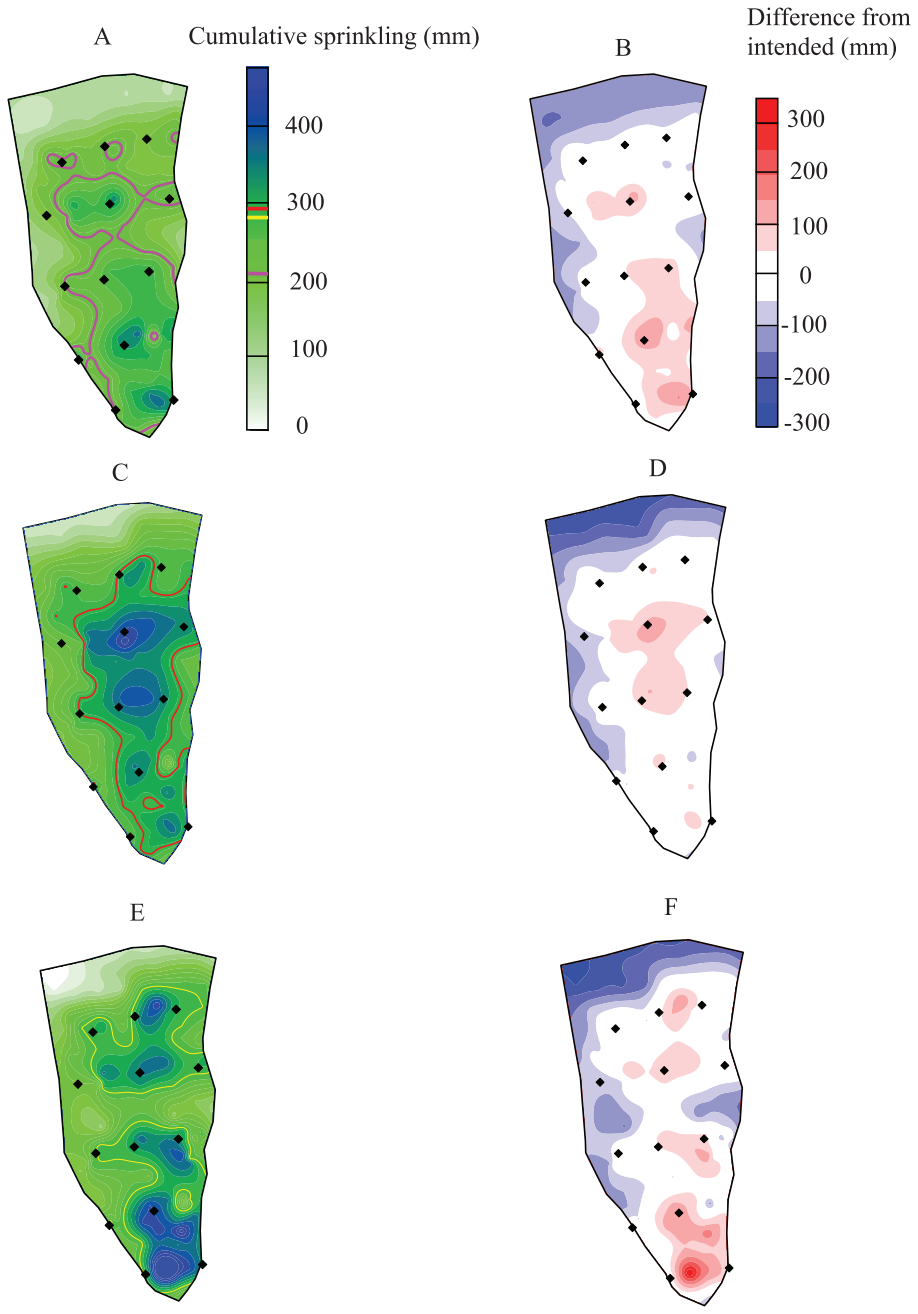

Fig. 9. (A) Cumulative sprinkling observed during experiment 1, the pink line in A and in the scale bar at 213 mm represents the intended cumulative rainfall (see table 2). (B) Difference between the intended cumulative rainfall for experiment 1 and the observed cumulative rainfall. (C) Cumulative rainfall observed during experiment 2, the red line in C and in the scale bar at 291 mm represents the intended cumulative rainfall (see table 2). (D) Difference between the intended cumulative rainfall for experiment 2 and the observed cumulative rainfall. (E) Cumulative rainfall observed during experiment 3, the yellow line in E and in the scale bar at 274 mm represents the intended cumulative rainfall (see table 2). (F) Difference between the intended cumulative rainfall for experiment 3 and the observed cumulative rainfall.

ET cannot be determined and was taken to be uniform. The consistency of sprinkling CU and CV values between day (active ET) and night (little to no ET) measurements (table 5) suggests that this approximation is reasonable.

Conceptual Model of ET

Sprinkling presents a unique scenario of meteorological conditions for the processes associated with ET. The driving forces for ET are inputs of energy (from the sun or atmosphere) and controls on the rate that energy (in the form of water vapor) can diffuse from the surface (Shuttleworth, 1991). The predominantly sunny conditions at CB1 during the sprinkling experiments provide a strong input of radiant energy from the sun, while at the same time the sprinkling provides a large amount of available water for evaporation and transpiration. In contrast to the meteorological conditions during natural precipitation, moisture originates from sprinklers mounted 2 m above the land surface. The sprinklers create a boundary-layer of high relative humidity from the height of sprinkling to the ground surface. The small vapor pressure gradient between the sprinklers and the vegetation canopy (less than 1.0 m in height) limit ET from the surface. The large vapor pressure gradient between the nearly-saturated air at the sprinkler height and the zone of drier air above the height of sprinkling drives evaporation of airborne droplets and mist. The most dominant of the lumped processes constituting ET during the sprinkling experiment is evaporation of airborne droplets and mist, which prevents a large portion of the sprinkling from reaching the land surface. The effective sprinkling, which is the input into the physics-based hydrologic response model in the companion paper (Ebel and others, 2007), is the amount reaching the surface observed in the manual rain gages. Estimation of ET and a water balance between the sprinklers and rain gages for experiment 3 are used to demonstrate this conceptual model.

Estimating ET

Estimation of ET in this study employs the Penman-Monteith method (P-M) (Monteith, 1965). The P-M equation can be expressed (Shuttleworth, 1993) as:

$$\mathrm{ET} = \frac{1}{\lambda} \frac{\Delta(R_N - G) + \dfrac{c_p \rho_a (e_s - e_a)}{r_a}}{[\Delta + \gamma(1 + r_c / r_a)]} \tag{3}$$

where ET is the evapotranspiration rate (mm d^{-1}), λ is the latent heat of vaporization (MJ kg^{-1}), Δ is the gradient of the saturation vapor pressure (kPa $C^{\circ -1}$), γ is the psychometric constant (kPa $C^{\circ -1}$), R_N is the net radiation (mm d^{-1}), G is the heat flux conducted into the soil (mm d^{-1}), c_p is the specific heat of air at constant pressure (J kg^{-1} $C^{\circ -1}$), r_a is the aerodynamic resistance to water vapor diffusion ($s^{-1}m$), e_s is the saturation vapor pressure (kPa), e_a is the ambient vapor pressure (kPa), r_c is the canopy resistance ($s^{-1}m$), and ρ_a is the air density (kg m^{-3}). It is worth noting that the units of R_N and G in equation (3) are mm d^{-1} water equivalent. The conversion from MJ m^{-2} d^{-1} to mm d^{-1} is 0.408 for water at 20 °C. All the relations used in this study to approximate the parameters for equation (3) that were not explicitly measured at CB1 are presented in Appendix A. For the special case of no canopy resistance, equation (3) reduces (Shuttleworth, 1993) to:

$$\mathrm{PET} = \frac{\Delta(R_N - G) + \dfrac{c_p \rho_a (e_s - e_a)}{r_a}}{\lambda[\Delta + \gamma]} \tag{4}$$

where PET (mm d^{-1}) is the potential evapotranspiration rate without any stomatal control on transpiration. During the sprinkler experiments when the plant surface is

continually wet as a result of constant sprinkling, the approximation represented by equation (4) is physically justifiable. However, before and after the sprinkling occurs the ET shifts from the height of sprinkling down to the vegetation canopy. The stomatal resistance of vegetative canopy then plays a dominant role in determining the ET flux. Because no porometer measurements were made at CB1 to parameterize the stomatal resistance term in equation (3), ET estimates using equation (4) are confined to times of minimal stomatal control.

Figure 5 shows a time series of the P-M ET estimates during the third sprinkling experiment. The diurnal trends of net radiation, temperature, and relative humidity produce a diurnal trend in the estimated ET rates. The estimated rates and diurnal trends in ET in figure 5 are consistent throughout experiment 3, with a mean P-M ET rate during the daylight hours of experiment 3 of 0.27 mm hr^{-1}. Higher ET rates on 5/31/1992 and lower ET rates on 6/1/1992 can be explained by differences in the relative humidity and air temperatures. For 5/31/1992, the air temperatures at 3.1 and 4.1m are 4 to 5 C° higher and the relative humidity is (on average) 20 percent lower during the daytime hours than for the previous 4 days of the experiment. For 6/1/1992, the air temperatures at 3.1 and 4.1 m are 2 to 3 C° lower while the relative humidity is (on average) 25 percent higher during the daytime hours than on the previous 4 days of the experiment, which is consistent with observations that noted enhanced cloud cover at CB1 on 6/1/1992 (Torres, ms, 1997).

Connections Between ET and Sprinkling

Figure 5 and previous observations (Montgomery and others, 1997) indicate that wind redistributes, and in some cases removes, sprinkling water from CB1. The amount of sprinkling that infiltrates is also reduced by ET. To examine the relative roles of wind and ET in sprinkling redistribution / removal, a water balance was conducted from the tank to the rain gages. The water mass balance from the sprinklers to infiltration (Seginer and others, 1991) is:

$$Q_{sprinkler} = Q_{drift} + Q_{evaporation} + Q_{infiltrating} \quad (5)$$

where $Q_{sprinkler}$ ($L^3\ T^{-1}$) is the application rates leaving the sprinklers determined from the water level decline in the tank, Q_{drift} ($L^3\ T^{-1}$) is the water carried off the catchment by wind, $Q_{evaporation}$ ($L^3\ T^{-1}$) is the water evaporated while the drops are airborne, and $Q_{infiltrating}$ ($L^3\ T^{-1}$) is the water that infiltrates. There are three assumptions needed for closure of the CB1 water balance in equation (5): (i) there were no transmission losses through the pipes from the tank to the sprinklers, (ii) $Q_{evaporation}$ is effectively estimated by equation (4), and (iii) $Q_{infiltrating}$ is the mean observed sprinkling rate (during the time of observation). The drift losses in equation (5) are estimated as the residual. For this study, $Q_{evaporation}$ was set to zero during the night and equal to the P-M ET estimates during the day. Sixteen measurements of $Q_{sprinkler}$ during experiment 3 reveal that 55 percent of the applied water infiltrated. The drift represented 39 percent of $Q_{sprinkler}$.

The largest contributing factor to drift is wind velocity, although sprinkler pressure also contributes to drift because higher pressures create smaller drop sizes that are more easily advected off-site (Yazar, 1984; Tarjuelo and others, 2000). The relatively high proportion of drift observed at CB1 is likely the result of the high wind velocities, frequently exceeding 4 m s^{-1} and peaking from 7:00 to 8:30 PM (fig. 5). It is worth pointing out that sprinkling tests were conducted at the field site prior to the three experiments and measured sprinkling rates in the network of 148 manual rain gages were used to calibrate sprinkling system to account for the drift losses, which results in the close agreement between the mean observed and intended sprinkling rate. Combining the conceptualization represented by equation (5) with the way the sprinkler tests were conducted, the sum of $Q_{infiltrating}$ per unit area (that is, the mean

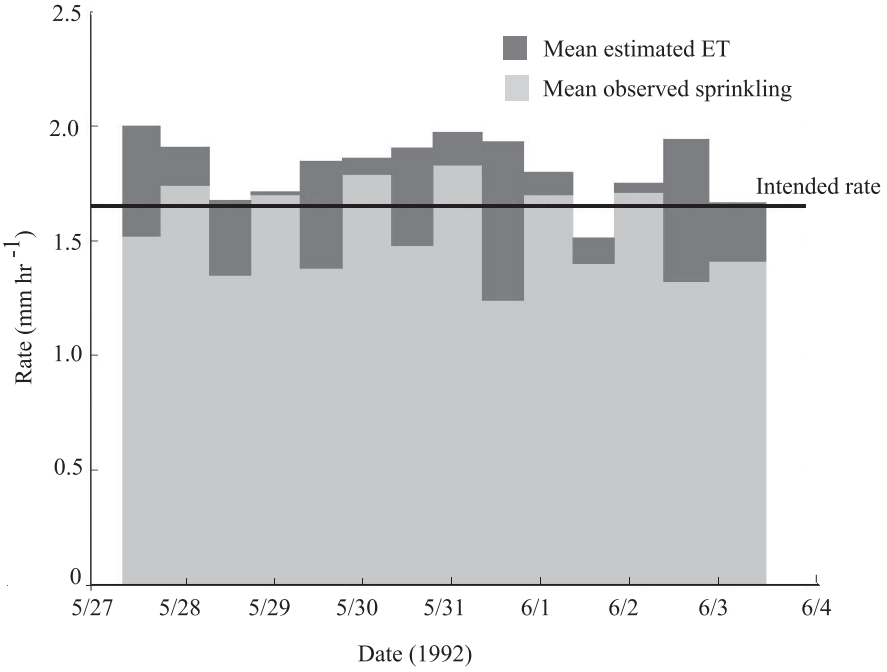

Fig. 10. Time series of mean observed sprinkling rate, mean estimated ET rate (using Penman-Monteith) over the same duration as the sprinkling measurements, and the intended sprinkling rate for experiment 3. The ET rate is corrected to allow comparison of the ET and sprinkling fluxes from the planimetric area.

observed sprinkling rates) and the ET rates per unit area should approximately equal the intended sprinkling rate (table 1). Figure 10 shows a time series of the sum of the mean estimated P-M ET rate (during the time of the sprinkling rate observations) and the mean observed sprinkling rate for experiment 3. Figure 10 illustrates that the conceptual model of sprinkling / ET interaction used for CB1 in this study is reasonable.

CONCEPTUAL HYDROGEOLOGIC MODEL

CB1 Geology and Soil

Bedrock at CB1 consists of volcaniclastic sandstone of Eocene age from the Flournoy Formation (Baldwin, 1974). Information on the physical characteristics of the sandstone bedrock is provided by a 35 m drill core at the ridge crest (Anderson and others, 2002). Porosity in the bedrock core (using bulk density and grain density) was 0.12 m^3 m^{-3} ($\pm$ 0.03), not including secondary porosity from fractures (Anderson, ms, 1995). Very limited data on fracture densities and apertures in the bedrock are available from CB1. Slight oxidation staining occurs at depths up to 24 m below the surface. This 24 m depth corresponds to the annual maximum depth to the water table observed in the onsite observation well where the 35 m core was taken (Anderson and others, 1997b). Above the unweathered bedrock, lies fractured, slightly-oxidized bedrock in a layer 3 to 4 m thick at the ridge crest, thinning downslope and pinching out at the channel head. Between the soil and the weathered bedrock, fractured saprolitic bedrock is present and well-developed near the ridge crest (up to 0.5 m thick), thinning downgradient towards the channel head where it pinches out (Ander-

TABLE 6

Characteristics of the CB1 saturated hydraulic conductivity (K_{sat}) estimates for the soil and bedrock using the Bouwer and Rice (1976) method

	K_{sat} (m s^{-1})		
Characteristic	Soil	Saprolite	Weathered bedrock
Arithmetic mean	1.1×10^{-4}	7.2×10^{-5}	1.7×10^{-5}
Geometric mean	6.2×10^{-5}	2.0×10^{-5}	1.7×10^{-6}
Standard deviation	8.6×10^{-5}	1.0×10^{-4}	2.7×10^{-5}
Median	1.0×10^{-4}	3.7×10^{-5}	1.4×10^{-6}
Minimim	4.0×10^{-8}	3.1×10^{-8}	5.4×10^{-8}
Maximum	4.8×10^{-4}	4.8×10^{-4}	9.9×10^{-5}
Number of estimates[1]	118	37	22

[1]The number of estimates does not include repeated measurements at the same location that are not included in the statistics.

son and Dietrich, 2001). While little soil profile information exists for the CB1 site, soil pits 70 m off-site reveal that the soil is a highly porous (0.5 - 0.6 m^3 m^{-3}) sandy loam (Torres, ms, 1997). The colluvial soil exhibits substantial small scale variability in soil depth (fig. 3B). The soil contains Mountain beaver (*Aplodontia rufa)* burrows ~0.2 m in diameter reaching 1.2 to 2.0 m depth (Torres and others, 1998). Burrow networks can extend up to 100 m in length with openings every 6 to 7 m (Schmidt, ms, 1999).

Slug Tests

Slug tests were performed at CB1 during the third sprinkling experiment consisting of 177 falling head slug tests in piezometers emplaced in the colluvial soil, saprolite, and weathered bedrock. The piezometer design at CB1 is described by Montgomery and others (1997). Results and conclusions from the CB1 slug tests are discussed in detail by Montgomery and others (2002). For the effort reported herein and the companion paper (Ebel and others, 2007), the slug test data were reanalyzed using the Bouwer and Rice (1976) method. Table 6 provides a statistical summary of the CB1 saturated hydraulic conductivity estimates. The values in table 6 are similar to those reported by Montgomery and others (2002) and support their conclusions. The statistical differences between the saturated hydraulic conductivity estimates in table 6 and the values reported by Montgomery and others (2002) are likely the result of, for this study, separating the saprolite estimates from the weathered bedrock and soil estimates, which is consistent with the geologic characterization by Anderson and Dietrich (2001). Slug test interpretation also has a subjective element relative to the choosing of the normalized response time (see Butler, 1998) that can affect saturated hydraulic conductivity estimates.

Montgomery and others (2002) examined the variation in saturated hydraulic conductivity estimates with depth and found: (i) an inverse relationship between piezometer depth and saturated hydraulic conductivity estimates within the soil and (ii) no discernable relation between piezometer depth and saturated hydraulic conductivity in the bedrock piezometers. The findings of Montgomery and others (2002) are in agreement with the saturated hydraulic conductivity estimates presented herein plotted as a function of depth. While consistent with observations from other studies that observed a decline in saturated hydraulic conductivity with depth in soils, (Beven, 1984; Elsenbeer and others, 1992; Ambroise and others, 1996), the correlation at CB1 is too weak to develop a reliable quantitative relationship between saturated hydraulic

conductivity and depth below the surface (Montgomery and others, 2002). It is worth noting that the gaps in the spatial distribution of the soil slug test data, particularly in the top 0.5 m of soil, prevent a meaningful 3D interpolation of the soil saturated hydraulic conductivity estimates. The lack of spatial structure and the small number (see table 6) of slug tests in the saprolite and weathered bedrock does not allow for a meaningful 3D interpolation of the saturated hydraulic conductivity.

EFFECTS OF SPRINKLING SPATIAL VARIABILITY ON HYDROLOGIC RESPONSE

Results from Previous Hydrologic Response Investigations at CB1

During the three sprinkling experiments, piezometric, tensiometric, and discharge measurements were taken repeatedly (see table 2). TDR measurements of soil-water content were also taken during the third experiment. Deuterium was introduced into the sprinkling water during the third experiment for tracer experiments in the vadose zone and concentrations were monitored using lysimeters (ceramic cup, tension, and plate). Discharge collected at the two weirs was analyzed for deuterium and bromide. Previous analyses of the CB1 data have advanced the understanding of hydrologic-response in steep, unchanneled valleys. For example, the major findings from Anderson and others (1997a), Montgomery and others (2002), Montgomery and Dietrich (2002) and Torres and others (1998) include: (i) the unsaturated zone delays the timing of pore-water pressure development and runoff generation, (ii) flow paths at the soil-saprolite-bedrock interface are important for runoff generation at CB1 (that is, subsurface storm flow), (iii) shallow bedrock fracture flow can control pore-water pressure magnitudes at CB1, (iv) the extremely high hydraulic conductivities in the soil (relative to the underlying bedrock) and steep slopes do not favor overland flow runoff generation mechanisms. The effects of spatial variations in sprinkling intensity have not been incorporated into the previous analyses of near-surface hydrologic response at CB1, except in the estimation of deuterium velocities by Anderson and others (1997b). The effort reported herein examines the effect of sprinkling spatial variability (see figs. 6, 7, 8, and 9; table 5) on the observed CB1 hydrologic response.

Effect of Spatial Variability in Sprinkling

Sprinkling variability effects in the near-surface.—Figures 11A, 11B, and 11C combine observations from piezometers and tensiometers to examine saturation in the soil during the three sprinkling experiments. Saturation is defined as when the pressure head is greater than zero for more than one consecutive tensiometer measurement or when pressure head in a piezometer is greater than 0.03 m, which is the height of the PVC cap on the bottom of the piezometers (Montgomery, ms, 1991). The saturated areas in figures 11A, 11B, and 11C are interpreted based on the saturated tensiometer and piezometer locations. Figures 11A, 11B, and 11C show the piezometers and tensiometers that were saturated at any time throughout the entire sprinkling experiment and are not intended to represent a snapshot of saturation at a given time. Because the piezometers and tensiometers are distributed vertically throughout the soil column, figures 11A, 11B, and 11C do not necessarily reflect saturation at the soil-saprolite interface. It is worth noting that piezometer analysis at CB1 indicates that saturation and pore-water pressure development are controlled primarily by fracture flow in the weathered bedrock and convergent subsurface flow (Montgomery and others, 1997).

The intended depth contour and the saturated area in figure 11A for experiment 1 do not correspond well, which may be the result of the small sprinkling depths / rates (see table 1, fig. 9A). However, some areas of inferred saturation in figure 11A do correspond with areas of anomalously high sprinkling depth shown in figures 9A and

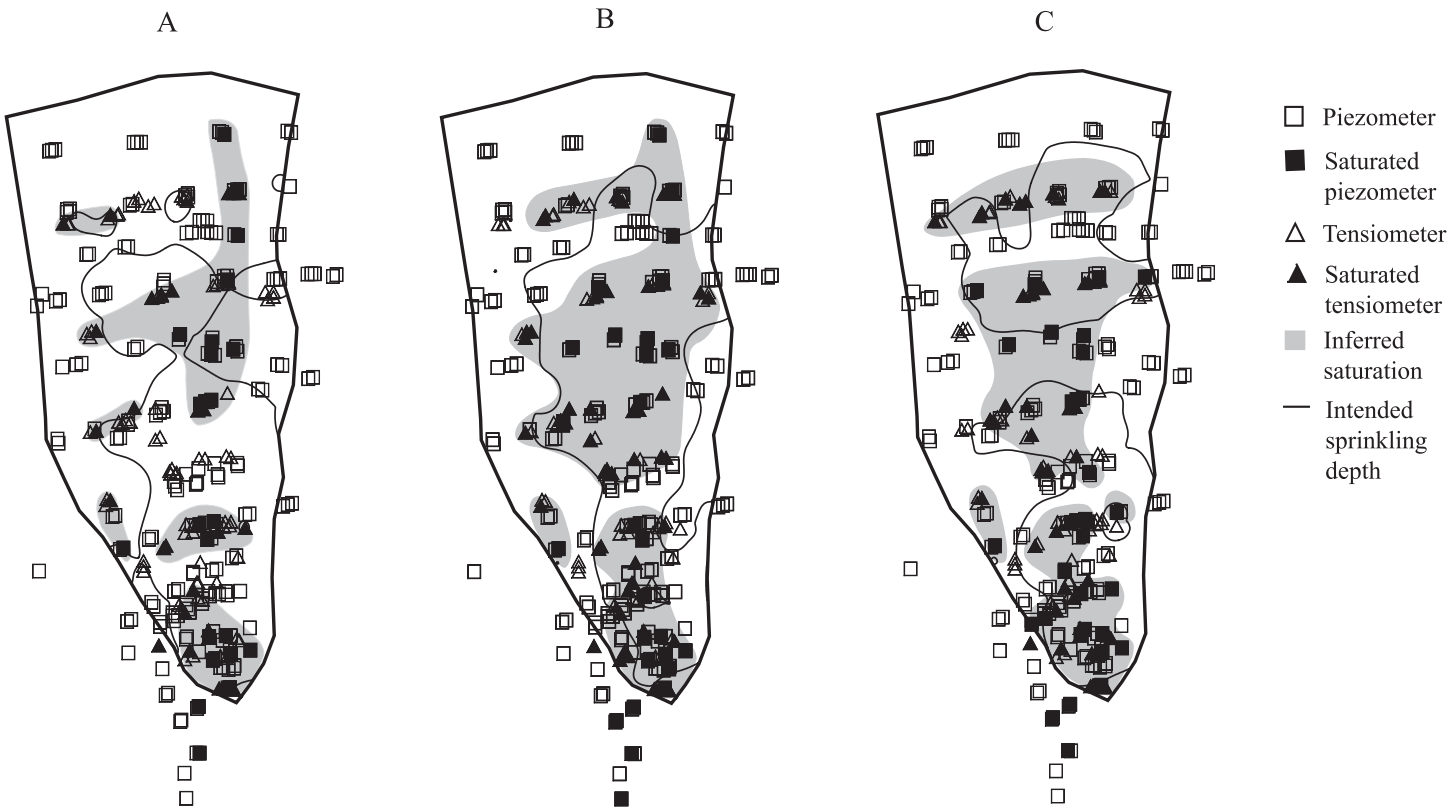

Fig. 11. Maps of inferred areas of saturation (shaded) based on piezometers and tensiometers (filled boxes and triangles). (A) Saturation map for experiment 1, the black contour line corresponds to the intended sprinkling depth (the pink line in fig. 9A). (B) Saturation map for experiment 2, the black contour line corresponds to the intended sprinkling depth (the red line in fig. 9C). (C) Saturation map for experiment 3, the black contour line corresponds to the intended sprinkling depth (the yellow line in fig. 9E).

9B. For example, the saturated areas near the middle of platforms 9, 7 and 5 (see fig. 3A) and near the left edge of platforms 11, 7 and 5 (see fig. 3A) correspond with high sprinkling depths shown in figures 9A and 9B. Comparison of figure 11A with previously reported saturation maps using piezometers (see Montgomery and others, 1997) reveals that the saturated areas are similar (patchy and discontinuous), but with additional information gained by considering tensiometer data.

Figure 11B for sprinkling experiment 2 illustrates a stronger correlation between the intended sprinkling depth contour and the area of inferred saturation. This correlation is most likely the result of the higher sprinkling rates in experiment 2. The saturated areas in figure 11B are less patchy than in figure 11A and nearly continuous along the surface and subsurface hollow axes (figs. 3A and 3B). Comparison of inferred saturation to sprinkling depths (figs. 9C and 9D) shows areas of saturation developing near elevated sprinkling depths near the middle of platforms 11, 9, 7, and 5 (fig. 3A) and near the left side of platforms 7 and 5 (fig. 3A). Comparison of the previous saturation maps from piezometers alone (see Montgomery and others, 1997) to figure 11B again reveals the additional information gained from considering tensiometer data.

Figure 11C represents the interesting "compromise" of experiment 3 compared to experiments 1 and 2 where the intended sprinkling depth in experiment 3 is almost equal to that of experiment 2 because of the longer duration while the intended sprinkling rate is close to that of experiment 1 (table 1 and fig. 9). Visually, the correlation between the contour of intended sprinkling depth and the inferred saturated area (fig. 11C) is not as strong as in experiment 2 (fig. 11B), but still significant and more prominent than for experiment 1 (fig. 11A). Comparisons of the areas of concentrated sprinkling from figures 9E and 9F to the saturated areas in figure 11C suggest that sprinkling heterogeneity can effect saturation development, for example the saturated areas along platforms 11 and 9, near the middle of platforms 7 and 5, and close to the left edge of platform 5 (fig. 3A).

Examination of figure 11C shows a gap in saturation between platforms 11 and 9 (see fig. 3A) along the hollow axis in experiment 3, despite the connected contour of intended depth. This suggests that the spatial continuity of sprinkling depth does not have a large impact on the continuity of the area of subsurface saturation along the hollow axis. It is worth repeating that figures 11A, 11B, and 11C represent the entire soil column and do not reflect saturation at the soil-saprolite interface nor do they represent a snapshot of saturation at a specific point in time. Instead, figures 11A, 11B, and 11C are indicative of saturation that develops within the soil column relative to spatial and temporal variations in sprinkling intensity. In particular, the saturation noted in the shallow tensiometers along platform 11 only lasts for several hours during experiment 1, 2, and 3 following locally elevated sprinkling intensities at those locations.

Spatial variability in tensiometric response was examined by Torres and others (1998) and no clear spatial pattern of the time to quasi-steady state, using an approach from Horton (1940), was found for sprinkling experiments 1 and 2. The timing to quasi-steady state for tensiometric response is defined herein, for experiment 3, as the first instance of consecutive decreasing pressure heads after the full arrival of the wetting front (that is, when pressure heads become near steady state). Figures 12A and 12B show overlays of the tensiometer time to quasi-steady state values at the 0.25 m ($\pm$ 0.05 m) and 0.5 m ($\pm$ 0.1 m) depths onto the Kriged sprinkling rates from the first 46 hours of experiment 3. The areas of higher sprinkling rates and the areas of more rapid time to quasi-steady state in figures 12A and 12B correspond. Some of the rapidly responding tensiometers are located near the left edge of platform 7 (fig. 3A) where sprinkling rates are small, which is likely the result of the shallow soils at those

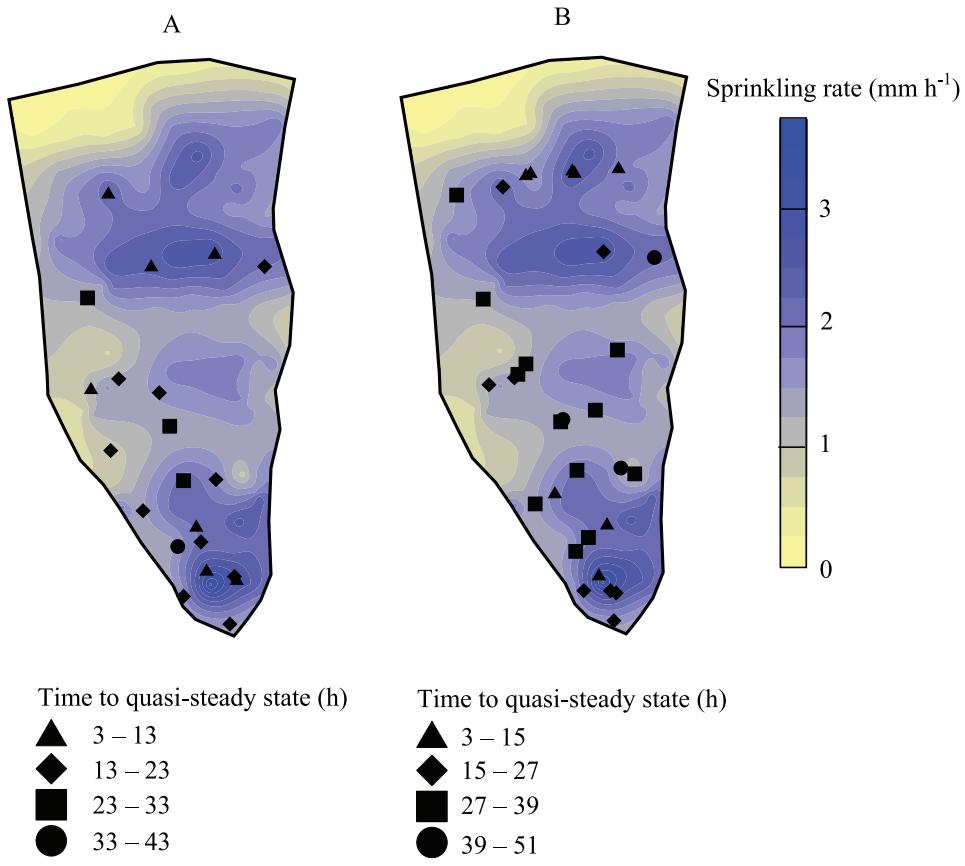

Fig. 12. Kriged sprinkling rates for the first 46 hours of sprinkling experiment 3 with the time to quasi-steady state from the tensiometer data at two depth intervals. (A) 21 observations of time to quasi-steady state at 0.25 m ± 0.1 depth. (B) 31 observations of time to quasi-steady state at 0.5 m ± 0.1 depth.

tensiometers (see fig. 3B). Overall, figures 12A and 12B suggest that sprinkling rates affect the timing to quasi-steady state for the tensiometers in experiment 3 and explain some of the observed spatial patterns of tensiometric response.

Sprinkling spatial variability effects at the soil-saprolite-bedrock interface.—Pore-water pressures and saturation at the soil-saprolite interface at CB1 could depend on spatial and temporal variations in sprinkling intensity / depth. Kriged maps of pore-water pressures from piezometers and tensiometers were created using the relation:

$$p = \rho g \psi \tag{6}$$

where p is the pore-water pressure (Pa), ρ is the density of water (kg m^{-3}), g is gravity (m s^{-2}), and Ψ is the pressure head (m). Piezometers are capable of observing pore-water pressures above zero and tensiometers are capable of observing pore-water pressures above and below zero (Harr, 1977; Johnson and Sitar, 1990).

Figures 13A, 13B, and 13C are snapshots at the time of peak pore-water pressure for experiments 1, 2 and 3, respectively, estimated using equation (6) and the observed pressure heads from the deepest piezometers and tensiometers from each nest (those closest to the soil-saprolite interface). The black contour line in figures 13A, 13B, and

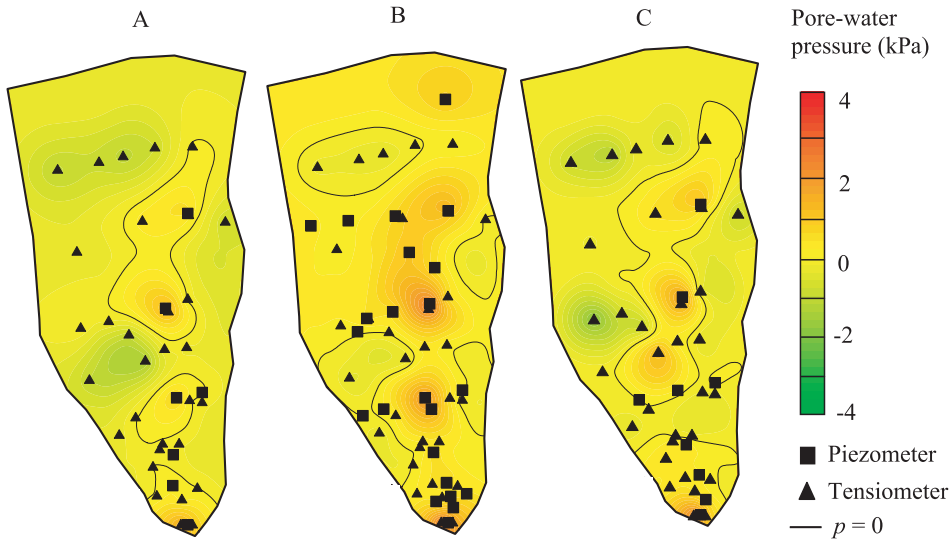

Fig. 13. Kriged snapshots of pore-water pressures based upon data from the piezometers and tensiometers closest to the soil-saprolite interface. (A) Peak pore-water pressures from experiment 1 at 10:00 PM on 5/13/1990. (B) Peak pore-water pressures from experiment 2 at 9:00 AM on 5/27/1990. (C) Peak pore-water pressures from experiment 3 at 10:00 AM on 5/31/1992.

13C marks the line of saturation (pore-water pressure equal to zero) at the soil-saprolite interface at the time of peak pore-water pressure. Comparison of figures 11A, 11B, and 11C to figures 13A, 13B, and 13C reveals the difference between saturation at any location throughout the soil column at any time during the experiment compared to saturation at the soil-saprolite interface at a specific point in time (snapshot). Figures 13A and 13C show that saturation is primarily developed near the hollow axis of the soil-saprolite interface (see fig. 3B). The saturation development (figs. 13A and 13C) is likely the result of convergent subsurface flow (Anderson and Burt, 1978; Montgomery and others, 1997; Freer and others, 2002), during experiments 1 and 3. Figure 13B shows that saturation at the soil-saprolite interface during the second sprinkling experiment develops near the subsurface hollow axis (fig. 3B) but extends over a larger area than figures 13A and 13C. In Figure 13B there are undoubtedly Kriging artifacts in areas where there is less data that show saturation reaching the ridge crest and at the left boundary that are not real. The saturated areas in figures 13A and 13C compare well with the saturated areas shown by Montgomery and others (1997, 2002), with additional understanding gained by considering tensiometer data.

Figures 13A, 13B, and 13C also suggest that pore-water pressure magnitudes may be affected by sprinkling intensity, which is consistent with field and laboratory observations (for example, Johnson and Sitar, 1990; Marui and others, 1993; Reid and others, 1997). For example the pore-water pressure hotspots in figures 13A, 13B, and 13C along the middle of platforms 9, 7 and 5 (see fig. 3A) correspond with areas of concentrated sprinkling in figures 9A, 9C, and 9E.

Effect of Sprinkling Spatial Variability on Water Balance Calculations

Several water-balance calculations have been conducted for the CB1 sprinkling experiments (see Anderson, ms, 1995; Montgomery and others, 1997; Torres, ms, 1997) using a variety of techniques to approximate the fluxes into and out of the catchment. Only the water balance of Torres (ms, 1997) considered spatially variable

input (sprinkling) and storage by dividing up the catchment into 5 areas for calculating spatially variable sprinkling and unsaturated soil-water storage (using TDR water contents) and incorporated the piezometer data to calculate saturated soil storage. A critical difference between the previously reported water balances and the one reported herein for experiment 3 is the use of all the observed manual rain gage data (and the corresponding exclusion of ET). If the observed sprinkling rate is equivalent to the intended sprinkling rate less the ET (as suggested by fig. 10), then the amount of water entering the catchment subsurface is approximately the same in the water balance reported here as in the previous studies (albeit not uniformly distributed in space).

The water balance results for this study represent the spatial variability in soil-water storage by combining nearby piezometer and tensiometer nests to produce pressure head profiles of the soil. Thirty piezometer / tensiometer groups were selected and the catchment was divided, with Thiessen (Voronoi) polygons, around those groups. The soil depth from the deepest piezometer in each group was then used to approximate the soil depth across the entire polygon. Interpolation between the observed pressure heads from the tensiometers and piezometers provided an estimate of the pressure head with depth profile for each polygon. The estimated pressure head profiles were converted to soil-water contents using the van Genuchten (1980) method and numerically integrated with respect to soil depth to give water content (m) for each polygon. When multiplied by the area of the polygon, the volume of water stored results. This calculation was made at the start of sprinkling experiment 3 (5/27/1992, 10:00 AM) and after the sprinkling experiment had ended when discharge from both the upper and lower weirs was almost zero (6/7/1992, 11:15AM). The calculated storages were 186 m^3 and 201 m^3 at the start and end of the experiment, respectively. A check of the water contents from the interpolation of the piezometer and tensiometer data using measured soil-water contents from nearby TDR data (where available) were only different (the mean of the absolute values of all the estimated minus observed soil-water contents) by 0.04 [m^3 m^{-3}] at the start of the third experiment. Unfortunately, no TDR data are available on 6/7/1992 to check the estimated soil-water contents at the end of the experiment. The difference between the starting and ending soil-water storage estimates indicates that approximately 15 m^3 of water was left in storage in the soil four days after sprinkling ended.

Using the estimate of stored soil water, it is possible to calculate the water balance for experiment 3 as:

$$I - R - (L + \Delta S_b) - \Delta S_s = 0 \tag{7}$$

where I is the irrigation [m^3] (sprinkling), R is the runoff [m^3], L is the leakage [m^3] to a regional groundwater system, ΔS_b is the change in saprolite and bedrock storage [m^3], ΔS_s is the change in soil storage [m^3]. The principal assumption employed in equation (7) is that deep leakage is closely linked with the amount of water going to bedrock storage. Equation (7) can be rearranged to solve for the combined term of deep leakage / bedrock storage as the residual in the water balance. The cumulative volume of water from the experiment 3 Kriged sprinkling total in figure 9E is 215 m^3, the cumulative runoff is 129 m^3, and the soil-water storage at the end of the water balance period is 15 m^3, yielding a residual of 71 m^3. Dividing the 71 m^3 residual by the duration of the water balance period, 265.25 hours, and then dividing by the planimetric area of the catchment gives an estimate of the rate at which water goes into bedrock storage / leaks of 8.7 x 10^{-8} m s^{-1} or 0.31 mm h^{-1}. The bedrock storage / leaking rate calculated herein using equation (7) of 0.31 mm h^{-1} is approximately equal to the deep leakage rate calculated by Anderson and Dietrich (2001) of 0.32 mm h^{-1}. Assuming a unity hydraulic gradient, the leakage rate provides a first-order estimate of the

saturated hydraulic conductivity of the deep bedrock. Although the methodology employed herein is slightly different than that employed in previous CB1 water balances, the incorporation of spatial variability in sprinkling and soil-water content does not significantly change the water balance calculation.

DISCUSSION

Data limitations exist in some the hydrologic-response analyses reported here. For example, capturing the spatial variations in sprinkling necessitates using the manual rain gage data, despite the limited temporal resolution. Previous research at CB1 suggests that small-scale temporal variations in sprinkling can significantly affect hydrologic response (Torres and others, 1998). However, the results presented here illustrate that spatial variability in sprinkling affects hydrologic response and that the sprinkling rates from the higher temporal resolution automated gages (see fig. 5) are inaccurate due to undercatch. The evaluation of natural rainfall variability relative to sprinkling variability was only analyzed for two natural storms and three sprinkling experiments; more research on this subject would further identify the differences between sprinkling and rainfall and how to account for / approximate these differences in analysis and simulation of hydrologic response. An additional limitation is the spatial distribution of saturated hydraulic conductivity estimates in the subsurface that prevents meaningful spatial interpolation. For example, bedrock saturated hydraulic conductivity variations at CB1 can control pore-water pressure generation (Montgomery and others, 1997), but spatial variations in saturated hydraulic conductivity were not included in the analyses presented here.

There are also limitations to the methods employed herein. One potential weakness is the reliance on Kriging to provide realistic interpolated values of different hydrologic observations (for example, rainfall depths / intensities, soil depths, and pore-water pressures). The drawbacks of Kriging include that it (i) has a tendency to smooth variations in the data (loses roughness), (ii) does not perform well in areas where there is little data (see the areas of saturation in fig. 13B near the ridgeline), (iii) relies on the semivariogram to provide an accurate portrayal of data structure, and (iv) produces only one realization of the interpolated attribute. However, visualization of spatially variable attributes requires some method of interpolation and, when provided with enough data (such as 148 rain gages), Kriging provides a reliable quantitative characterization. When less data is available (30 or so points across the entire CB1 catchment), we have qualified our results by explicitly stating that the interpolation is best viewed in a qualitative sense. For example, it would be unwise to use Kriged pore-water pressure snapshots, like those shown in figures 13A, 13B, and 13C, to drive a 3D slope stability assessment. Another potential weakness of the method employed in this paper is the limited physical representation of the P-M ET method relative to the meteorological complexity of the sprinkling experiments. For example, the input of sprinkling water with a different (but unknown) temperature than the air is a significant complication to the energy balance used to formulate the P-M method. However, the data does not exist to apply more complicated ET models at CB1 and the P-M method represents most of the energy balance correctly.

Previous field and modeling studies have suggested that convergent surface and subsurface topography is the dominant controlling factor of saturation and pore-water pressure generation (for example, Anderson and Burt, 1978; Sidle and others, 1985; Mirus and others, 2007). Examination of figures 3A and 3B and figures 9A, 9B, 9C, 9D, 9E, and 9F illustrates that areas of high sprinkling depths / intensities are concentrated along the surface and subsurface hollow axes. The collocation of the hollow axes and elevated sprinkling depths prevents definitively separating the magnitude of the hydrologic effects of convergent subsurface flow and sprinkling heterogeneity at CB1. However, it is still clear that sprinkling heterogeneity affects hydrologic response,

although likely to a lesser extent than convergent subsurface flow. It is worth noting that if the saturation is perched at the soil-saprolite interface (or another impeding layer below), then that saturation development depends critically on the sprinkling rate because if the sprinkling is less than the saturated hydraulic conductivity of the perching layer, then no saturation will develop.

The major conclusions from previous work at CB1 remain unchanged by the effort reported here. Instead, some of the nuances of hydrologic-response were examined with respect to sprinkling spatial variability. Quantitative spatial analyses of the observed CB1 hydrologic response provide the foundation for the physics-based hydrologic-response simulations reported in the companion paper (Ebel and others, 2007).

SUMMARY

The analyses presented herein indicate that simulated rainfall is more spatially variable than natural storms at CB1 and that detailed spatial characterization of sprinkling intensity is worthwhile. Experimental semivariograms of sprinkling rates offer a more comprehensive measure of spatial variability and continuity than either univariate statistics (such as the CU, CV, and SD) or more qualitative methods of spatial variability (such as contour maps of interpolated rates). Reproducing the spatial characteristics (that is, continuity, structure, and variance) of natural rainfall at a given study site is a useful benchmark for evaluating rainfall simulators. Careful measurement of the sprinkling depths at CB1, combined with ET estimation, allows the effective rainfall (with ET losses already removed) to be approximated by the amount observed in the manual rain gages. The CB1 water balance calculations were not significantly changed by incorporating spatial variability in sprinkling rates or soil-water storage. Both tensiometric response and saturation within the CB1 near-surface soil profile are affected by sprinkling heterogeneity. Pore-water pressure and saturation development deep in the CB1 soil (at the soil-saprolite-bedrock interface) are more sensitive to convergent flow driven by subsurface topography, but are still sensitive to sprinkling spatial heterogeneity. Previous analyses (Montgomery and others, 1997) demonstrate that pore-water pressure generation is also affected by bedrock saturated hydraulic conductivity variations controlled by fracture locations. Spatial variability in sprinkling rates should be incorporated into hydrologic-response models designed to predict subsurface saturation and pore-water pressure development when employed in physics-based simulation of hydrologic response of sprinkling experiments, such as the effort reported in the companion paper (Ebel and others, 2007).

ACKNOWLEDGMENTS

The work reported herein was supported by National Science Foundation Grant EAR-0409133. The presentation in this paper has benefited from the thoughtful comments of Steve Loheide, Steve Burges, Ben Mirus, Chris Heppner, and Adrianne Carr. Jef Caers provided valuable insight into geostatistical analysis. Kevin Schmidt supplied additional data on the soil and saprolite depths. Obviously, the research reported herein and in the companion paper would not have been possible without the data collection at CB1 more than a decade ago, which was greatly facilitated by John Heffner. The clarity of the paper was improved by the comments of Keith Beven and two anonymous reviewers.

APPENDIX

The latent heat of vaporization (MJ kg^{-1}) was approximated as a function of the water temperature (T_s), in C°, as (Harrison, 1963):

$$\lambda = 2.501 - 0.002361(T_s) \tag{A1}$$

The saturation vapor pressure gradient (Δ) was approximated (Tetens, 1930), in kPa °C^{-1}, as:

$$\Delta = \frac{de_s}{dT} = \frac{4098e_s}{(237.3 + T)^2} \tag{A2}$$

where T is the air temperature (°C). The saturation vapor pressure (kPa) was approximated as a function of air temperature (Tetens, 1930) as:

$$e_s = 0.6108 \exp\left(\frac{17.27T}{237.3 + T}\right) \tag{A3}$$

The psychometric constant (kPa °C^{-1}) is given (Brunt, 1952) by:

$$\gamma = 0.0016286 \frac{P}{\lambda} \tag{A4}$$

where P is the atmospheric pressure in kPa. The density of air (kg m^{-3}) was estimated as a function of temperature and pressure (Smith and others, 1992) as:

$$\rho_a = 3.486 \frac{P}{T_{KV}} \tag{A5}$$

where T_{KV} is the virtual temperature (°K) and was approximated (Smith and others, 1992) as:

$$T_{KV} = 1.01(T_a + 273) \tag{A6}$$

The ambient vapor pressure was estimated using the assumption that relative humidity is equivalent to the ratio of the actual vapor pressure to the equilibrium vapor pressure at saturation (Brutsaert, 1982), which was estimated , in kPa, as:

$$e_a = \frac{RH}{100}(e_s) \tag{A7}$$

The aerodynamic resistance (ra) was estimated (Shuttleworth, 1993), in s m^{-1}, as:

$$r_a = \frac{\ln[(z_u - d)/z_{0m}]\ln[(z_e - d)/z_{0h}]}{k^2 u_z} \tag{A8}$$

where z_u and z_e are the heights of the wind and humidity measurements, respectively (m), z_{om} is the roughness length for momentum transfer (m), z_{oh} is the roughness length for heat and water vapor transfer (m), d is the zero plane displacement height (m), k is the von Karman constant (-) (approximated as 0.41), and u_z is the wind velocity (m s^{-1}). The zero plane displacement height (m) was estimated empirically using the relationship (Brutsaert, 1982) as:

$$d = 0.67h \tag{A9}$$

where h is the vegetation height (m). The windspeed profiles were measured at heights larger than d, and an equation using windspeeds at two heights, z_1 and z_2 was used to calculate the roughness length for momentum transfer (Monteith and Unsworth, 1990) as:

$$z_{0m} = \exp\left[\frac{u_2 \ln z_1 - u_1 \ln z_2}{u_2 - u_1}\right] \tag{A10}$$

where u_1 and u_2 are wind velocities (m s^{-1}) measured parallel to the slope at heights z_1 and z_2 (m). The roughness length for water vapor and heat transfer (z_{Oh}) was approximated (Brutsaert, 1982) as:

$$z_{0h} = \frac{z_{0m}}{\exp(B^{-1}k)} \tag{A11}$$

where B^{-1} is a resistance parameter that depends on the roughness of the surface vegetation. The B^{-1} parameter was approximated as 2.0 for short vegetation (Brutsaert, 1982).

REFERENCES

Ambroise, B., Beven, K., and Freer, J., 1996, Toward a generalization of the TOPMODEL concepts: topographic indices of hydrologic similarity: Water Resources Research, v. 32, p. 2135–2145.
Anderson, M. G., and Burt, T. P., 1978, The role of topography in controlling throughflow generation: Earth Surface Processes and Landforms, v. 3, p. 331–344.
Anderson, S. P., ms, 1995, Flow paths, solute sources, weathering, and denudation rates: The chemical geomorphology of a small catchment: Berkeley, California, University of California, Berkeley, Ph. D. thesis, University of California, 380 p.
Anderson, S. P., and Dietrich, W. E., 2001, Chemical weathering and runoff chemistry in a steep headwater catchment: Hydrological Processes, v. 15, p. 1791–1815.
Anderson, S. P., Dietrich, W. E., Torres, R., Montgomery, D. R., and Loague, K., 1997a, Concentration discharge relationships in runoff from a steep, unchanneled catchment: Water Resources Research, v. 33, p. 211–225.
Anderson, S. P., Dietrich, W. E., Montgomery, D. R., Torres, R., Conrad, M. E., and Loague, K., 1997b, Subsurface flowpaths in a steep, unchanneled catchment: Water Resources Research, v. 33, p. 2637–2653.
Anderson, S. P., Dietrich, W. E., and Brimhall, G. H., 2002, Weathering profiles, mass-balance analysis, and rates of solute loss: Linkages between weathering and erosion in a small, steep catchment: GSA Bulletin, v. 114, p. 1143–1158.
Ascough, G. W., and Kiker, G. A., 2002, The effect of irrigation uniformity on irrigation water requirements: Water South Africa, v. 28, p. 235–242.
Baldwin, E. M., 1974, Eocene stratigraphy of southwestern Oregon: Bulletin of the Oregon Department of Geology and Mineral Industries, v. 83, p. 1–38.
Beven, K. J., 1984, Infiltration into a class of vertically nonuniform soils: Hydrologic Sciences Journal, v. 29, p. 425–434.
Bouwer, H., and Rice, R. C., 1976, A slug test for determining hydraulic conductivity of unconfined aquifers with completely or partially penetrating wells: Water Resources Research, v. 12, p. 423–428.
Brunt, D., 1952, Physical and dynamical meteorology, 2nd edition: Cambridge, University Press, p. 428.
Brutsaert, W., 1982, Evaporation into the atmosphere: Theory, history, and applications: Dordrecht, Holland, Reidel Publishing, 299 p.
Butler, J. J., Jr., 1998, The design, performance, and analysis of slug tests: New York, Lewis Publishers, 252 p.
Christiansen, J. E., 1942, Irrigation by sprinkling: California Agricultural Experiment Station Bulletin, n. 670.
Croke, J., Hairsine, P., and Fogarty, P., 1999, Runoff generation and re-distribution in logged eucalyptus forests, south-eastern Australia: Journal of Hydrology, v. 216, p. 56–77.
Ebel, B. A., and Loague, K., 2006. Physics-based hydrologic-response simulation: Seeing through the fog of equifinality: Hydrological Processes, v. 20, p. 2887–2900.
Ebel, B. A., Loague, K., VanderKwaak, J. E., Dietrich, W. E., Montgomery, D. R., Torres, R., and Anderson, S. P., 2007, Near-surface hydrologic response for a steep, unchanneled catchment near Coos Bay, Oregon: 2. Comprehensive physics-based simulations: American Journal of Science, v. 307, p. 709–748.
Elsenbeer, H., Cassel, K., and Castro, J., 1992, Spatial analysis of soil hydraulic conductivity in a tropical forest catchment: Water Resources Research, v. 28, p. 3201–2143.
Esteves, M. E, Planchon, O., Lapetite, J. M., Silvera, N., and Cadet, P., 2000, The 'EMIRE' large rainfall simulator: design and field testing: Earth Surface Processes and Landforms, v. 25, p. 681–690.
Freer, J., McDonnell, J. J., Beven, K. J., Peters, N. E., Burns, D. A., Hooper, R. P., Aulenbach, B., and Kendall, C., 2002, The role of bedrock topography on subsurface storm flow: Water Resources Research, v. 12, p. 1269–1284.
Gilbert, G. K., 1877, Report on the geology of the Henry Mountains: Washington, D. C., Government Printing Office, 170 p.
Hall, M. J., 1970, A critique of methods of simulating rainfall: Water Resources Research, v. 6, p. 104–1114.
Harr, R. D., 1977, Water flux in soil and subsoil on a steep forested slope: Journal of Hydrology, v. 33, p. 37–58.
Harrison, L. P., 1963, Fundamental concepts and definitions relating to humidity, *in* Wexler, A., editor, Humidity and Moisture, v. 3: New York, Reinhold Publishing Company, p. 3–70.
Hornberger, G. M., Germann, P. F., and Beven, K. J., 1991, Throughflow and solute transport in an isolated sloping soil block in a forested catchment: Journal of Hydrology, v. 124, p. 81– 99.
Horton, R. E., 1940, An approach towards the physical interpretation of infiltration-capacity: Soil Science Society of America Proceedings, v. 5, p. 399–417.
Johnson, K. A., and Sitar, N., 1990, Hydrologic conditions leading to debris-flow initiation: Canadian Geotechnical Journal, v. 27, p. 789–801.
Kincaid, D. C., 1996, Spraydrop kinetic energy from irrigation sprinklers: Transactions of the ASAE, v. 17, p. 839–845.
Lane, P. N. J., Croke, J., and Dignan, P., 2004, Runoff generation and burnt convergent hillslopes: rainfall simulation and modeling: Hydrological Processes, v. 18, p. 879–892.
Lascelles, B., Favis-Mortlock, D. T., Parsons, A. J., and Guerra, A. J. T., 2000, Spatial and temporal variation in two rainfall simulators: implications for spatially explicit rainfall simulation experiments: Earth Surface Processes and Landforms, v. 25, p. 709–721.
Loch, R. J., Robotham, B. G., Zeller, L., Masterman, N., Orange, D. N., Bridge, B. J., Sheridan, G., and Bourke, J. J., 2001, A multi-purpose rainfall simulator for field infiltration and erosion studies: Australian Journal of Soil Research, v. 39, p. 599–610.

Luk, S. H., Abrahams, A. D., and Parsons, A. J., 1983, Sediment sources and sediment transport by rill flow and interrill flow on a semi-arid piedmont slope, Southern Arizona: Catena, v. 20, p. 93 –111.
Marui, A., Yasuhara, M., Kuroda, K., and Takayama, S., 1993, Subsurface water movement and transmission of rainwater pressure through a clay layer, *in* Gladwell, J. S., editor, Hydrology of Warm Humid Regions: Wallingford, United Kingdom, IAHS Press, v. 216, p. 463–470.
Mirus, B. B., Ebel, B. A., Loague, K., and Wemple, B. C., 2007, Simulated effect of a forest road on near-surface hydrologic response: redux: Earth Surface Processes and Landforms, v. 32, p. 126–142,
Monteith, J. L., 1965, Evaporation and environment: The State and Movement of Water in Living Organisms, Symposium of the Society for Experimental Biology, n. 19, p. 205-234.
Monteith, J. L., and Unsworth, M. H., 1990, Principles of environmental physics: New York, Edward Arnold, 291 p.
Montgomery, D. R., ms, 1991, Channel initiation and landscape evolution : Berkeley, California, University of California, Berkeley, Ph. D. thesis, 421 p.
Montgomery, D. R., and Dietrich, W. E., 2002, Runoff generation in a steep, soil-mantled landscape: Water Resources Research, v. 38, p. 1168–1175.
Montgomery, D. R., Dietrich, W. E., Torres, R., Anderson, S. P., Heffner, J. T., and Loague, K., 1997, Hydrologic response of a steep, unchanneled valley to natural and applied rainfall: Water Resources Research, v. 33, p. 91–109.
Montgomery, D. R., Dietrich, W. E., and Heffner, J. T., 2002, Piezometric response in shallow bedrock at CB1: Implication for runoff generation and landsliding: Water Resources Research, v. 38, p. 1274–1292.
Motha, J. A., Wallbrink, P. J., Hairsine, P. B., and Grayson, R. B., 2002, Tracer properties of eroded sediment and source material: Hydrologic Processes, v. 16, p. 1983–2000.
Newson, A. J., and Clarke, R. T., 1976, Comparison of the catch of ground-level and canopy-level rain-gauges in the Upper Severn Experimental Catchment: Meteorological Magazine, v. 105, p. 2–7.
Parsons, A. J., Stromberg, S. G. L., and Greener, M., 1998, Sediment-transport competence of rain-impacted interill overland flow: Earth Surface Processes and Landforms, v. 23, p. 365– 375.
Reid, M. E., LaHusen, R. G., and Iverson, R. M., 1997, Debris flow initiation experiments using diverse hydrologic triggers, *in* Chen, C. L., editor, Debris Flow Hazards Mitigation: Mechanics, Prediction and Assessment, ASCE Proceedings, p. 1–11.
Riley, S. J., and Hancock, F., 1997, A rainfall simulator for hydrologic and erosion experiments on mines, with an example of its applications at Ranger Uranium Mine, Northern Territory, Australia: The Australasian Institute of Mining and Metallurgy Proceedings, v. 1, p. 3–8.
Rodda, J. C., and Smith, S. W., 1986, The significance of systematic error in rainfall measurement for assessing wet deposition: Atmospheric Environment, v. 20, p. 1059–1064.
Schmidt, K. M., ms, 1999, Root strength, colluvial soil depth, and colluvial transport on landslide-prone hillslopes: Seattle, Washington, University of Washington, Seattle, Ph. D. thesis, 258 p.
Seginer, I., Kantz, D., and Nir, D., 1991, The distortion by wind of the distribution patterns of single sprinklers: Agricultural Water Management, v. 19, p. 341–359.
Sharpley, A., and Kleinman, P., 2003, Effect of rainfall simulator and plot scale on overland flow and Phosphorus transport: Journal of Environmental Quality, v. 32, p. 2172–2179.
Shuttleworth, W. J., 1991, Evaporation models in hydrology, *in* Schmugge, T. J., and André, J., editors, Land surface evaporation : measurement and parameterization: New York, Springer Verlag, p. 93–120.
——— 1993, Evaporation, *in* Maidment, D., editor, Handbook of Hydrology: New York, McGraw Hill Publishers, p. 4.1– 4.53.
Sidle, R. C., Pearce, A. J., and O'Loughlin, C. L., 1985, Hillslope stability and land use: Washington D. C., American Geophysical Union, Water Resources Mongraph, v. 11, 140 p.
Smith, M., Allen, R. G., Monteith, J. L., Perrier, A., Pereira, L., and Segeren, A., 1992, Report of the expert consultation on procedures for revision of FAO guidelines for prediction of crop water requirements: UN-FAO, Rome, Italy, 54 p.
Sumner, H. R., Wauchope, R. D., Truman, C. C., Dowler, C. C., and Hook, J. E., 1996, Rainfall simulator and plot design for mesoplot runoff studies: Transactions of the American Society of Agricultural Engineers, v. 39, p. 125–130.
Tarjuelo, J. M., Ortega, J. F., Montero, J., and de Juan, J. A., 2000, Modelling evaporation and drift losses in irrigation with medium size impact sprinklers under semi-arid conditions: Agricultural Water Management, v. 43, p. 263–284.
Taylor, G., Hale, C., and Joos, S., 2005, Climate of Coos County, Special report, Oregon Climate Service: Corvallis, Oregon, Oregon State University, p. 1–4.
Tetens, O., 1930, Uber einige meteorologische Begriffe*:* Zeitschrift für Geophysik, v. 6, p. 297–309.
Torres, R., ms, 1997, Unsaturated zone processes and the hydrologic response of a steep, unchanneled valley: Berkeley, California, University of California, Berkeley, Ph. D. thesis, 298 p.
Torres, R., Dietrich, W. E., Montgomery, D. R., Anderson, S. P., and Loague, K., 1998, Unsaturated zone processes and the hydrologic response of a steep, unchanneled catchment: Water Resources Research, v. 34, p. 1865–1879.
van Genuchten, M. Th., 1980, A closed-form equation for predicting the hydraulic conductivity of unsaturated soils: Soil Science Society of America, v. 44, p. 892–898.
Waddington, J. M., and Devito, K. J., 2001, Portable irrigation system for studying hillslope and wetland runoff generation processes: Hydrological Processes, v. 15, p. 281–287.
Wilson, C. J., 1999, Effects of logging and fire on runoff and erosion on highly erodible granitic soils in Tasmania: Water Resources Research, v. 35, p. 3531–3556.
Wisler, C. O., and Brater, E. F., 1959, Hydrology: New York, John Wiley, 408 p.
Yazar, A., 1984, Evaporation and drift losses from sprinkler irrigation systems under various operating conditions: Agricultural Water Management, v. 8, p. 439–449.